Structure and Dynamics of Solid Polymers from 2D- and 3D-NMR

H. W. SPIESS

Max-Planck-Institut für Polymerforschung, Postfach 3148, D-6500 Mainz, FRG

Received February 15, 1991 (Revised Manuscript Received June 25, 1991)

Contents

H. W. Spiess received his Ph.D. in physical chemistry at the University of Frankfurt, Germany, with H. Hartmann in 1968. After a two year's postdoctoral stay at Florida State University with R. K. Sheline, he returned to Germany and joined the staff of the Max-Planck-Institute, Department of Molecular Physics at Heidelberg under the direction of K. H. Hausser. In 1975 he changed to the Chemistry Department of the University at Mainz, where he became a Professor in 1978. After professorships at the Universities of Münster (1981–82) and Bayreuth (1983–84) he was appointed as a director at the newly founded Max-Planck-Institute for Polymer Research in Mainz. His main research interests are development of solid-state NMR techniques for the study of structure and dynamics of synthetic polymers and liquid crystalline systems.

I. Introduction

The macroscopic properties of polymeric materials depend on the structure, order, and dynamics of the macromolecular chains.[1–3] Therefore, a variety of physicochemical techniques has been applied in order to characterize these properties.[4–5] Among these, nuclear magnetic resonance (NMR) has proven particularly powerful and versatile.[6,7] The most important advantage of NMR is its selectivity, which can be achieved in two ways:

High-resolution NMR in solids, in particular of ^{13}C in natural abundance. The improved resolution together with an enhancement of signal intensity is achieved[8] by a combination of $^{1}H/^{13}C$ cross-polarization, high power proton decoupling, and magic-angle spinning (CPMAS-NMR). This technique by now is standard and its methodical background as well as numerous applications to solid polymers have been reviewed already.[7–15] The structural information that can be obtained from such ^{13}C NMR spectra is similar to that of liquid state ^{13}C NMR spectroscopy. The isotropic chemical shift is an indicator of the structural element to which the detected nucleus belongs and of the conformation of the molecule. In addition, line shape and spin relaxation can be exploited to yield valuable information about the phase behavior as well as the molecular dynamics.

Selective isotope labeling, in particular by deuterons, ^{2}H. This method offers a second route to achieve high selectivity. Although it involves an often laborious chemical synthesis, this technique has been widely applied in recent years not only in academia but also in industrial laboratories.[15–19] The importance of ^{2}H NMR comes from the fact that the spectral resolution that can be achieved by CPMAS-NMR is often not sufficient to resolve the sites of particular interest. Isotopic labeling by ^{2}H solves this problem and allows the orientation of the molecular sites to be monitored by a well-defined direction, namely the selected C–^{2}H bond. The analysis of ^{2}H NMR line shapes as well as various relaxation parameters thus provides unique information about molecular order and dynamics.

Recently, two-dimensional (2D) NMR techniques[20] have been introduced into this area as well. Multidimensional spectroscopy offers a number of advantages. First of all the introduction of a new frequency dimension increases the spectral resolution. This is particularly important in solid-state NMR, where the resolution is especially low, due to the presence of anisotropic interactions. However, multidimensional spectroscopy also provides additional information, unavailable from 1D spectra even in the limit of high

0009-2665/91/0791-1321$09.50/0

resolution. Experiments can be designed which correlate different spin interactions structural information or, through exchange, relate the various states taken up by the molecule during different time periods. These two types of experiments provide structural and dynamic information, respectively.

For slow and ultraslow motions 2D NMR[20] separates the information on the time constants from that on the geometry of the dynamic process under study.[21,22] The angular resolution is particularly high in ^{2}H NMR, but 2D exchange NMR has also been successfully applied to natural abundance ^{13}C NMR in static[23] and in rotating[23,24] solids. This makes it a versatile tool for studying slow dynamic processes in solid-state physics, polymer science, and biophysics.

Magic-angle spinning (MAS) increases the spectral resolution in ^{13}C NMR at the expense of angular resolution. For slow spinning speeds the centerbands at the isotropic chemical shifts are flanked by sidebands occurring at multiples of the rotor frequency.[9] While this complicates the MAS spectra, the sidebands can be used to study the anisotropy of the chemical shift, yielding important structural information. This information can, in fact, be obtained with greater resolution, if 2D techniques are employed that separate the isotropic from the anisotropic chemical shift.[20] The use of sideband patterns for the study of molecular motions was first demonstrated by Veeman et al.,[24] and the phase problems associated with 2D exchange NMR under MAS were solved by Hagemeyer et al.[23]

The determination of macroscopic as well as microscopic properties such as, e.g. conformational order in partially oriented fibers of synthetic and biopolymers, aligned liquid crystalline polymers, etc. represents another important area of current and future applications of 2D solid-state NMR. In fact, the periodic variation of the NMR signal resulting from the application of MAS to a partially ordered sample[25] provides a particularly easy way of generating a second frequency dimension[26] via rotor synchronization. This technique has been successfully applied to systems of varying degrees of complexity.[26]

Two-dimensional exchange spectroscopy can also be used to detect spin diffusion.[27] This offers a means to probe domain sizes and interfacial regions in heterogeneous polymers. In homogeneous polymer blends spin diffusion can detect mixing on a molecular level.[28,29] Spin diffusion is most efficient among protons. The spectral resolution of ^{1}H NMR in solids, however, often is not sufficient to discriminate between the different components in complex polymer systems, even under CRAMPS (combined rotation and multiple-pulse spectroscopy) conditions.[30] Here, ^{13}C detection of ^{1}H spin diffusion has opened up new possibilities.[31]

In this review the different techniques are described and illustrated using selected applications to synthetic polymers. As far as structural information is concerned emphasis is placed on methods which are useful for studying the structure of polymers on length scales that exceed 1 nm. Solid-state NMR techniques for elucidating internuclear distances or conformation of the monomer units are described only briefly. Of course, the techniques, can likewise be used to study structure and dynamics of biopolymers. Extended theoretical derivations are avoided. Only MAS-NMR is treated in more detail, since 2D MAS-NMR requires a slightly different theoretical background than readily available elsewhere. New developments that extend solid-state NMR to *three* dimensions are also included.

II. 1D Solid-State NMR

A. Basics

In the solid state molecules are much less mobile than in a liquid. Whereas anisotropic, angular dependent interactions are averaged out by the fast isotropic molecular motion in liquids,[6] they often dominate the NMR spectrum of solids.[7-10] Most common is the magnetic dipole–dipole coupling of the nuclei among themselves: homonuclear dipole–dipole coupling, e.g. ^{1}H–^{1}H, or heteronuclear, e.g. ^{1}H–^{13}C. In a conventional wide-line spectrum this dipole–dipole coupling leads to broad, featureless bands, which are difficult or impossible to analyze quantitatively. In order to obtain high-resolution NMR spectra of solids, the dipole–dipole coupling must be removed. Homonuclear and heteronuclear couplings require different decoupling schemes, namely multiple-pulse NMR and high power proton decoupling, respectively. The dipole–dipole interaction, on the other hand, is also exploited in solid-state NMR as a valuable source of information. It provides the mechanism for spin diffusion,[27] i.e. diffusion of magnetization through a solid without transport of material. This in turn allows one to check the proximity of different components in heterogeneous materials. In addition, the heteronuclear dipole–dipole coupling allows signal enhancement through cross-polarization, e.g. ^{1}H/^{13}C.

The magnetic shielding of the nuclei by the surrounding electrons, known in liquids as the chemical shift, is anisotropic in the solid state. Typically the powder patterns for carbons in different environments overlap and cannot be unraveled clearly. Therefore MAS is applied to achieve sufficient resolution. This technique makes use of the fact that the nuclear spin interactions are described by second-rank tensors.[9] Thus, fast rotation about an axis inclined at an angle ϕ with respect to the magnetic field scales the interaction by a factor $^1/_2\,(3\cos^2\phi - 1)$, which vanishes at the "magic angle" $\phi = 54.7°$. If the angular velocity ω_R of the spinning is substantially smaller than the spectral width of the powder pattern, the latter is split into sidebands occurring at multiples of ω_R on either side of the centerband, thus retaining valuable information about molecular order and dynamics. Shielding anisotropies are particularly pronounced for carbon atoms involved in π-bonds, e.g. aromatics and carbonyls,[9-11] with the resulting frequency shifts proportional to the strength of the external magnetic field. This is particularly important in the high-field instruments used today.

In addition to these magnetic interactions, nuclei with spin $I > ^1/_2$ can also have electric quadrupole moments. These lead to quadrupole coupling to the electric field gradient at the nuclear site.[9] This quadrupole coupling can, in fact, be comparable with or even stronger than the magnetic coupling with the external field. However, for ^{2}H (I = 1), in C–^{2}H bonds it leads to spectral splittings of ca. 250 kHz, which are of the same order as the splittings resulting from ^{1}H–^{1}H homonuclear

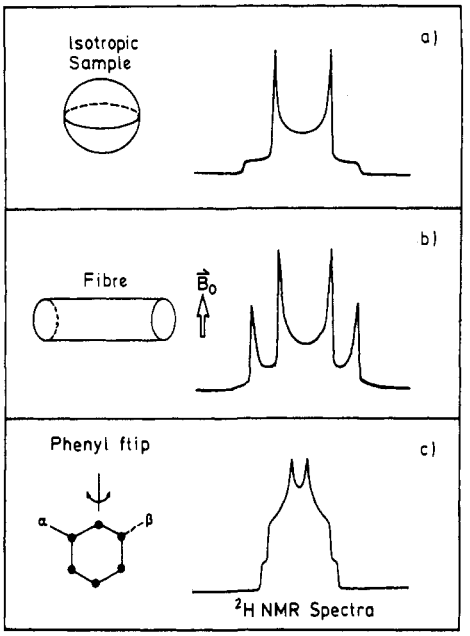

Figure 1. Calculated deuteron NMR line shapes: (a) rigid isotropic solid, (b) rigid drawn fiber, and (c) isotropic solid with flipping phenyl rings.

coupling (ca. 50 kHz), ^{1}H–^{13}C heteronuclear coupling (ca. 25 kHz), and frequency shifts due to the anisotropy of the chemical shift (ca. 15 kHz at a field strength of 7 T). Since C–H bonds are common in polymers ^{2}H labeling is particularly useful.

If one of the above-mentioned couplings dominates, either because of its strength, or because the others have been suppressed by decoupling, the angular dependence of the NMR frequency in high magnetic fields is alike for all couplings and is given by

$$\omega = \omega_L + \tfrac{1}{2}\Delta(3\cos^2\theta - 1 - \eta\sin^2\theta\cos 2\phi) \quad (1)$$

Here ω_L is the Larmor frequency, Δ describes the strength of the anisotropic coupling: i.e. anisotropic chemical shift or ^{13}C–^{1}H dipole–dipole coupling for ^{13}C, quadrupole coupling for ^{2}H, and η is the asymmetry parameter describing the deviation of the anisotropic coupling from axial symmetry ($0 \le \eta \le 1$). The angles θ and ϕ are the polar angles of the magnetic field $\vec{B}_0$ in the principal axes system of the coupling tensor. This in turn is often simply related to the molecular geometry: i.e. the unique axis being along a bond direction, e.g. dipole–dipole coupling, ^{13}C–^{1}H bond; quadrupole coupling, C–^{2}H bond, or perpendicular to a sp_2 plane as for ^{13}C chemical shift tensors in aromatic rings, etc. Depending on the total spin involved, signals described by eq 1 and their mirror images with respect to ω_L may be superimposed and in powder samples the spectra for all orientations are added to yield the powder lineshape (e.g., the Pake pattern for ^{2}H with spin $I = 1$).

The line shape of the static NMR spectra is an important source of information. Examples of ^{2}H NMR line shapes are presented in Figure 1. The three cases considered involve an isotropic powder (Pake pattern), a planar distribution of C–H bonds in a unaxially drawn fiber and a phenyl ring with motional averaging, due to flipping about the axis shown. The latter process first detected for side groups of amino acids[32] has been shown to be quite common in solid polymers and to be closely related with their mechanical properties, e.g. in bisphenol A polycarbonate.[33]

Spin–relaxation parameters provide another important source of information concerning molecular dynamics as well as the phase structure and the proximity of polymer chains in block copolymers and blends.[12] In addition to the longitudinal or spin–lattice relaxation that probes molecular motions at rates in the neighborhood of the NMR frequency itself, i.e. around 50–500 MHz, slower motions can be monitored via nuclear relaxation processes in the rf field of the spectrometer (i.e. ca. 1–50 kHz). Characteristic times for cross-polarization or transverse relaxation probe even slower processes.

The 2D and 3D methods described below are useful for elucidating ultraslow motions which are of particular interest in order to understand the mechanical properties of polymers. It should be mentioned, however, that line shape and relaxation experiments are widely used for examining faster motions in synthetic polymers as well as in other systems.[12-19,34]

B. Magic-Angle Spinning

To understand the literature on the 2D and 3D experiments described below some basic theory of MAS-NMR has to be appreciated. To this end we consider a single crystallite with only one type of carbon site and assume that the spectrometer transmitter frequency is set to the isotropic Larmor frequency ω_L. It is important to realize that MAS renders the Hamiltonian explicitly time-dependent. Following a $\pi/2$ pulse or cross polarization, the magnetization of a single spin packet, therefore, evolves with a time-dependent precession frequency $\omega(t)$.[35] The evolution of the magnetization can be described in terms of the angle $\vartheta(t_1, t_2)$ over which it rotates in the x,y plane of the rotating frame between times t_1 and t_2. This rotation angle is obtained from an integration over the instantaneous precession frequency $\omega(t)$

$$\vartheta(t_1,t_2) = \int_{t_1}^{t_2}\omega(t)\,dt = \Theta(t_2) - \Theta(t_1) \quad (2)$$

and can be written as the difference of the angles $\Theta(t_2)$ and $\Theta(t_1)$ that the magnetization vector forms with the x axis of the rotating frame at times t_2 and t_1, respectively.

To describe the behavior of the different crystallites and to permit treatment of partially ordered systems, cf. section V.A, several different coordinate systems are introduced in Figure 2. First a molecular frame (MF) is defined, which may be chosen at our convenience with respect to some arbitrary feature of the molecular geometry. For a partially oriented sample, it is necessary to define a frame of reference for the axis of preferential orientation, the director, henceforth denoted as the director frame (DF). It is related to the rotor frame of reference (RF), whose z axis is the spinning axis and whose y axis lies in the plane of the rotor axis and the director, by Euler angles (α_0, β_0, γ_0). Note that RF is a rotor fixed frame. It is related to the laboratory frame (LF), whose z axis is along the static external magnetic field and whose y axis lies in the plane of rotor axis and magnetic field, by Euler angles (Ψ, $\Theta_m = 54.7°$, $0°$). Therefore Ψ is time-dependent. It is clear from Figure 2 that $\Psi = \Psi_0 + \omega_R t$, where Ψ_0 specifies a particular rotor position, e.g. at the beginning of the experiment.

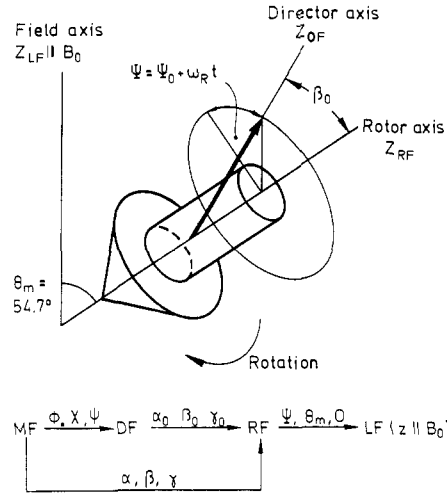

Figure 2. Definition of the angles β_0 and Ψ, which relate the sample axis to the rotor axis and the direction of the magnetic field B_0. The relationships between the four coordinate systems used to describe MAS experiments are also indicated.

The MF is related to rf by Euler angles (α, β, γ). Because RF is a rotor fixed frame, α, β, and γ are time-independent. Finally, MF and DF are related by Euler angles (ϕ, χ, ψ).

The contribution of the single crystallite to the free induction decay (FID) is then given by

$$g(t) = \exp\left[i\int_0^t \omega(t)\,dt\right] = \exp[i\Theta(t)]\exp[-i\Theta(0)] \equiv f[\gamma + \Psi(t)]\,f^*[\gamma + \Psi(0)] \quad (3)$$

with

$$f(\gamma) = \exp\{i[A\sin(2\gamma) - B\cos(2\gamma) + C\sin(\gamma) - D\cos(\gamma)]\} \quad (4)$$

These f functions depend on the Euler angles (α, β, γ) and on the components of the chemical-shift tensor σ as expressed in the MF, which are determined by the orientation of the chemical-shift tensor relative to the MF. Explicit expressions for the coefficients A, B, C, and D can be found elsewhere.[26] Introducing $\Psi = \Psi_0 + \omega_R t$ into eq 3 and dropping the constant rotor phase offset Ψ_0 we obtain

$$g(t) = f(\gamma + \omega_R t)f^*(\gamma) \quad (5)$$

In order to simplify the notation we keep only the dependence on the rotor phase in the argument list of the f functions, because this variable is essential for an understanding of the two-dimensional experiments to be discussed later. Note that the f functions are periodic with

$$f(\gamma + n\omega_R T_R) = f(\gamma + n2\pi) = f(\gamma) \qquad n \in N \quad (6)$$

T_R being the rotor period and n any integer. Thus the calculations can be confined to an interval of 2π. The Fourier transformation (FT) of any periodic function in time with period T_R leads to a frequency spectrum consisting of a set of sidebands spaced ω_R apart. To proceed further we have to calculate the sideband intensities. Herzfeld and Berger[36] have expressed all f functions by infinite sums over products of Bessel functions. For our purpose, we prefer to insert a δ function, as described by Mehring:[9]

$$1 = \frac{1}{2\pi}\int_0^{2\pi} d\vartheta\ \delta(\vartheta - \gamma - \omega_R t) \quad (7)$$

and then to expand the δ function in terms of plane waves

$$\delta(\vartheta - \gamma - \omega_R t) = \sum_N \exp[\pm iN(\vartheta - \gamma - \omega_R t)] \quad (8)$$

Thus eq 5 can be rewritten as

$$g(t) = f^*(\gamma)\int_0^{2\pi} d\vartheta\ \delta(\vartheta - \gamma - \omega_R t)\,f(\vartheta) = \sum_N \exp[iN\omega_R t]\exp[iN\gamma]\,f^*(\gamma)\int_0^{2\pi} d\vartheta\ \exp[-iN\vartheta]\,f(\vartheta) \quad (9)$$

where we have neglected a proportionality constant of 2π that accompanies the plane wave expansion. This does not bear any significance for the relative sideband intensities and common factors in similar situations can in general be discarded.

For an isotropic sample we must sum up all the contributions from crystallites with different orientations. Further, if we omit our assumption of on-resonance irradiation, then the evolution of the magnetization due to the isotropic chemical shift σ_i, has to be added. To account for transverse relaxation with time constant T_2 we multiply the MAS FID with an exponentially decaying function. This leads to the following expression for the time-domain signal of each carbon residue in a rotating sample:

$$G(t) = \sum_N \exp[i\omega_L\sigma_i t]\exp[iN\omega_R t]\int_0^{2\pi} d\gamma\ \exp[iN\gamma]\,f^*(\gamma)\int_0^{2\pi} d\vartheta\ \exp[-iN\vartheta]\,f(\vartheta)\exp[-t/T_2] = \sum_N \exp[i\omega_L\sigma_i t]\exp[iN\omega_R t]F^*_N F_N \exp[-t/T_2]$$

with

$$F_N = \int_0^{2\pi} d\vartheta\ \exp[-iN\vartheta]\,f(\vartheta) \quad (10)$$

In the absence of T_2 decay the FT of eq 10 would yield infinitely sharp sidebands (δ functions) centered at $\omega_N = \omega_L\sigma_i + N\omega_R$ and with intensities $I_N = F^*_N F_N$. However, because of T_2 relaxation (and perhaps additional damping) the sidebands are broadened. The line shape of individual sidebands is governed by the FT of the decay function, which in itself consists of absorptive and dispersive components. This causes severe phase problems in 2D MAS-NMR as discussed in detail in the appendix of ref 23. The 1D MAS spectrum of a powder sample, however, obtained from eq 10 by FT reads

$$I(\omega) = \sum_N [A(\omega - \omega_N) + iD(\omega - \omega_N)]F^*_N F_N \quad (11)$$

and can be phased to pure absorption mode by a standard linear phase correction routine, since $F^*_N F_N$ is a real and positive number.

III. Separation and Correlation of Interactions by 2D Techniques

A. Basics

The time scheme of two-dimensional solid-state NMR is identical with that of high-resolution 2D NMR

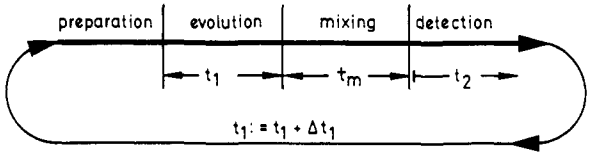

Figure 3. Time scheme of two-dimensional NMR.

spectroscopy of liquids[20] and is shown schematically in Figure 3. The spin system is first brought in to a well-defined initial state during the preparation period. The most common preparation consists of spin–lattice relaxation followed by a 90° pulse or cross-polarization. During the following evolution period t_1 the spin system develops under the influence of the various spin interactions introduced in section II. In conventional 1D NMR the nuclear signal is recorded during the time t_1 and the spectrum is produced by a subsequent FT. In 2D NMR spectroscopy, however, the state of the spin system after a certain time t_1 is altered abruptly by at least one further rf pulse. The signal is then recorded during a subsequent detection period (t_2). The entire experiment is repeated for a whole range of evolution times t_1. The 2D NMR spectrum is produced[20] by two successive FTs after t_2 and t_1. Finally, a mixing time t_m may be introduced between the evolution and the detection period (Figure 3) during which nuclear magnetization can be mixed between different states due to dynamic processes. As noted above, one of the goals of 2D NMR spectroscopy is to separate and correlate interactions. This section describes some examples of such experiments. A systematic overview of the various types of solid-state 2D NMR has been given elsewhere.[37]

B. Separation of Isotropic and Anisotropic Chemical Shifts

As noted above, information about the anisotropic chemical shift is retained in the sideband pattern of high-resolution MAS-NMR spectra of solids. For systems with a large number of chemically inequivalent sites and large anisotropies, 1D MAS is often insufficient because of overlapping sidebands. Several two-dimensional schemes have, therefore, been proposed in order to separate the isotropic component from the anisotropic interactions, including chemical shift scaling,[38] periodic sequences of π pulses,[39] and mechanical manipulations of the rotor.[40,41] Unfortunately, these techniques are technically demanding and none of them is completely successful in removing the anisotropies in one of the frequency dimensions.

Recently, a novel 2D experiment has been introduced in this area.[42] It utilizes the so-called TOSS (total suppression of spinning sidebands) sequence introduced by Dixon[43] and further analyzed by Griffin et al.[44] The TOSS sequence consists of four π-pulses with delays chosen such, that after applying TOSS to an isotropic powder, the spin system appears to evolve under the influence of the isotropic chemical shift much as if it were in solution. The careful phase alignment of the magnetization trajectories accomplished by TOSS can, however, be reversed. This is the basis of the experiment introduced by Kolbert and Griffin.[42] As shown in Figure 4, after applying TOSS the spin system evolves for the time t_1 and no sidebands appear in ω_1. Then the reverse TOSS sequence is applied, reintroducing the anisotropic chemical shifts during the detection period, such that along ω_2, isotropic and anisotropic chemical shifts are probed. The highly improved resolution obtained in this way is nicely demonstrated in the experimental example of ^{13}C NMR in tyrosine hydrochloride[42] (Figure 4). For actual applications it is important to note that the performance of TOSS can be improved substantially by phase cycling and by the use of composite pulses.[44]

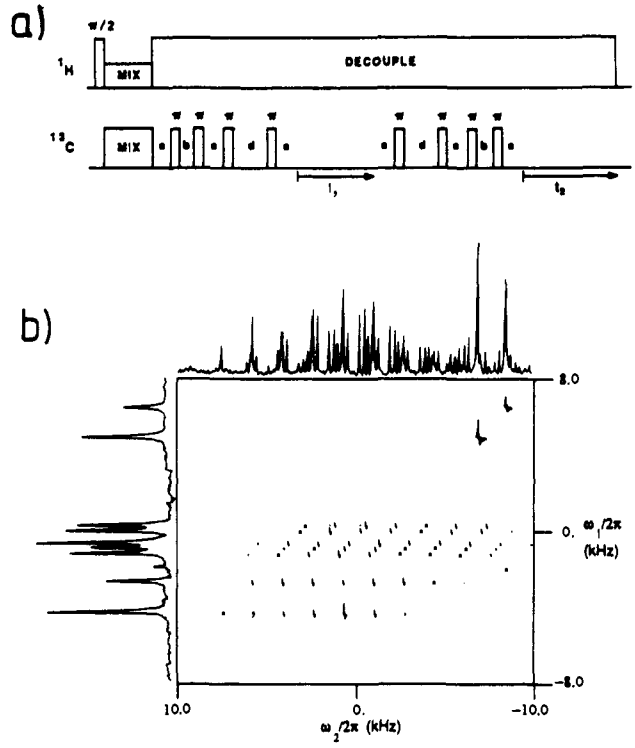

Figure 4. Separation of isotropic and anisotropic chemical shifts: (a) pulse sequence and (b) 2D ^{13}C MAS spectrum of Tyr–HCl. The conventional MAS spectrum is given on top, the ω_1-projection, free of sidebands, is plotted to the left (adopted from ref 42).

As mentioned above several schemes have been proposed to record two-dimensional spectra, where a MAS spectrum is recorded in one and powder patterns governed by anisotropic chemical shifts are recorded in the other. They all involve the application of π-pulses. A common feature of these versions is the fact that the powder patterns of the 2D spectra do not, in general, have the same shapes as 1D powder lineshapes of stationary samples. This complicates the data analysis. In a more recent scheme,[45] this restriction has been overcome by applying 4 or even 6 π pulses.

C. Correlation of Dipole–Dipole Couplings and Chemical Shifts

The dipole–dipole coupling, e.g. between ^1H and ^{13}C, or ^1H and ^{15}N, provides valuable structural information. Since the C–H and N–H bond lengths are known, the measurements of dipolar splittings can be interpreted in terms of the angles between individual bonds and the applied magnetic field. In order to be useful, the dipolar patterns have to be correlated, however, with the chemically distinct sites in a molecule or a monomer unit, i.e. with the chemical shift of the ^{13}C or ^{15}N nuclei. Since the dipolar couplings correspond to local fields, such experiments are often named "separated local field" (SLF) experiments as proposed by Waugh,[46] the

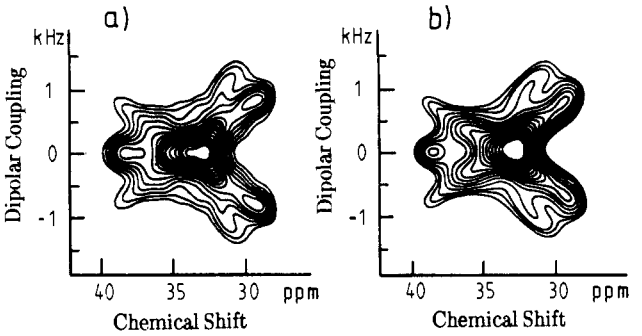

Figure 5. ^{13}C chemical shift/^{13}C-^{1}H dipolar 2D powder spectrum of polyethylene: (a) experimental and (b) simulated (adopted from ref 51).

pioneer of high-resolution NMR in solids. For static powder samples 2D SLF spectra display characteristic ridges from which the relative orientation of the chemical shift and the dipolar coupling tensors may be deduced.[47] Sideband patterns governed by ^{13}C–^{1}H dipolar couplings introduced by Munowitz et al.[48] have been used extensively in the past by Schaefer and co-workers to study molecular dynamics of polymers, in particular polystyrene and polycarbonate.[49] The application of SLF spectroscopy for structure determination in proteins has recently been reviewed.[50] To simplify the spectra, oriented fibers are used.

As a recent example of SLF spectroscopy in Figure 5 we present a 2D^{13}C chemical shift/$^{13}C^{1}H$ dipolar powder pattern of polyethylene.[51] Here the anisotropies are scaled by off-magic-angle spinning, where the rotation axis is 54.7° + 4° in the evolution and 54.7° + 14° in the detection period, respectively. During half of the evolution period the homonuclear ^{1}H–^{1}H dipolar interaction is removed by applying a multiple pulse sequence.[9] From the analysis of the 2D pattern the principal values of the ^{13}C chemical shift tensor, the C–H bond length and the H–C–H bond angle can be determined. The authors find better agreement between experimental and simulated 2D patterns assuming that the principal axes of the chemical shift tensor deviate slightly from the symmetry axes of the CH_2 group.

The measurement of small dipolar couplings for structural investigations, in particular of biopolymers either between nuclei that both have low magnetic dipole moments such as ^{13}C–^{13}C or ^{13}C–^{15}N or due to coupling to remote protons, requires special techniques. As discussed by Kolbert et al.,[52] hybrid experiments that combine the elements of spin-echo NMR, chemical-shift scaling, switched-speed MAS, etc. can achieve resolution and sensitivity that would be unattainable by any of these methods alone. Therefore such hybrid experiments provide superior information. New approaches in this area involve rotational echo double resonance (REDOR)[53] and the use of rotational resonances.[54]

IV. 2D Exchange NMR: Molecular Dynamics

A. Static Samples

Let us consider 2D exchange spectra of deuterons first, since a number of experimental examples are available already. It should be noted, however, that 2D exchange NMR has also been successfully applied to

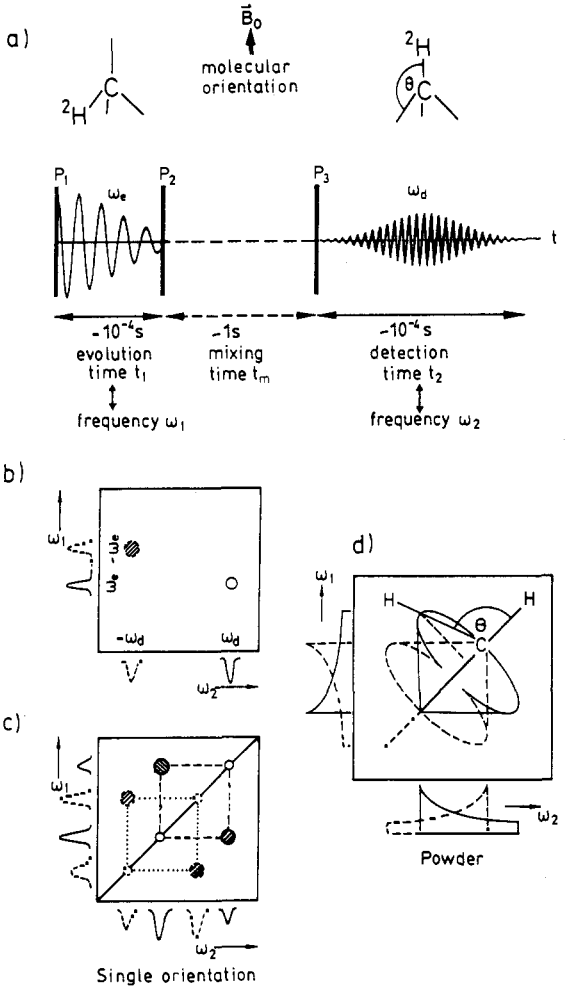

Figure 6. Two-dimensional exchange NMR and rotational motions: (a) three pulse sequence, (b) 2D exchange pattern for a single site in a single crystal, (c) 2D exchange spectrum for a single crystal and two NMR transitions (I = 1) as for ^{2}H, and (d) ^{2}H 2D exchange spectrum for a powder. A single reorientational angle θ is considered throughout.

spin $I = {}^1/_2$ nuclei such as ^{13}C, ^{31}P, etc.

In 2D exchange NMR a given ensemble of deuteron spins after a first pulse P_1, cf. Figure 6a, evolve with a frequency ω_e reflecting the molecular orientation at that time. Instead of generating a NMR spectrum by FT with respect to the evolution time t_1, the state of the spin system is stored by a second rf pulse P_2 and is read out again after the mixing time t_m by a third pulse P_3, which starts the detection period t_2.[21] If the molecular orientation has changed during t_m due to slow molecular reorientation, the deuteron spins will evolve with another frequency ω_d corresponding to the new molecular orientation. Note that t_m typically is substantially longer than t_1 or t_2. By repeating the experiment with an incremented value of t_1 a two-dimensional data set is generated, which after two subsequent FTs yields a 2D exchange NMR spectrum.[20]

In the absence of motion, the frequences ω_e and ω_d of a given ^{2}H spin in the evolution and detection periods, respectively, are the same and a signal along the diagonal of the spectrum is observed. In the *presence* of molecular reorientation on the time scale of t_m, the molecules can change their orientation during t_m and the NMR frequencies ω_e and ω_d will be different. This exchange leads to off-diagonal cross peaks in the 2D

spectrum, cf. Figure 6b. It demonstrates the Gedanken experiment that all C–^{2}H bonds have a single orientation corresponding to the frequency ω_e during t_1 and are changing by a jump through the angle Θ to another orientation connected with the frequency ω_d during t_2. On the two axes of the 2D spectrum the NMR spectra corresponding to the two molecular orientations before and after the mixing time, as shown in Figure 6b, are plotted. The reorientation leads to an exchange peak at the position $\omega_1 = \omega_e$ and $\omega_2 = \omega_d$. The second peak $(-\omega_e, -\omega_d)$ arises from the second transition of the spin $I = 1$ system. In reality there is an equal probability for the jump forward and backward, so that both frequencies occur in both, t_1 and t_2. This is reflected in the symmetry of the spectrum with respect to the main diagonal. The second transition of the spin $I = 1$ system leads to the mirror symmetry about the antidiagonal, so that the 2D exchange spectrum shows C_{2v} symmetry, cf. Figure 6c. From the frequency coordinates of the exchange peaks the orientation before and after the mixing time can easily be calculated with the help of eq 1. For an isotropic powder sample the exchange spectrum is not a single peak but a broad inhomogeneous pattern covering partially or even fully the 2D plane.

If all molecules rotate about the same well-defined angle, such that the C–^{2}H bond directions change by the angle Θ, the 2D exchange spectrum displays characteristic ridges in the form of ellipses,[21] given by the following parametric representation:

$$\omega_1 = \tfrac{1}{2}\Delta[1 + 3\cos 2\vartheta] \tag{11a}$$

$$\omega_2 = \tfrac{1}{2}\Delta[1 + 3\cos(2\vartheta \pm 2\Theta)] \tag{11b}$$

where ϑ serves as a parameter. Thus the so-called reorientational angle Θ is directly projected into the 2D spectrum and can be calculated from

$$|\tan\Theta| = b/a \tag{12}$$

where a and b are the principal axes of the ellipse, parallel and perpendicular to the diagonal of the spectrum, respectively. With the help of eq 3 it is possible to read the reorientational angle Θ directly with a ruler, cf. Figure 6d. Consequently there is no model involved in obtaining this geometric information about the motional mechanism.

It is important to realize that in general the reorientational angle Θ is not identical with the rotational angle of a polymer segment about a carbon–carbon bond or an average chain axis, etc. Instead, it measures the relative angle between C–^{2}H bonds (or C_3 axes of methyl groups) before and after the rotation. The different angles are, of course, interrelated through the geometry of the chain. When only a few reorientational angles are involved in a motional mechanism an equal number of ellipses is observed in the 2D exchange spectra. More complex motions lead to a distribution of reorientational angles. The exchange spectra of diffusive motions can thus be understood as superpositions of the spectra for an infinite number of reorientational angles. Consequently, when exchange is due to diffusive motion no sharp contours appear in the 2D exchange spectrum, but a new characteristic line shape is observed. In this way different reorientation mechanisms such as discrete jumps or small-step angular diffusion can be distinguished.

As an illustrative example let us consider two models often employed when simulating polymer dynamics: (1) chain motion in a diamond lattice and (2) chain motion by isotropic rotational diffusion. These two models, in fact, correspond to considerably different views of the molecular dynamics. Motion in a diamond lattice considers highly localized conformational transitions with fixed constraints[55] and involves rotations by a fixed angle $\Theta = 109.4°$, the tetrahedral angle. On the other hand rotational diffusion of a chain in the bulk can only be visualized as a cooperative process since it involves rotation by arbitrarily small angles. Relatively broad angular distributions can, however, also occur if Brownian motion and conformational transitions with flexible constraints are considered.[56,22]

The simulated 2D exchange spectra for the two models in the limit $t_m \gg \tau_c$, where τ_c is the correlation time of the respective process, are plotted in Figure 7. The ellipses due to the tetrahedral jump motion on the lattice (Figure 7a) can clearly be distinguished from the broad unstructured exchange signal reflecting the broad angular distribution due to rotational diffusion (Figure 7b). The inserts of Figure 7 show the even part of the reorientational angle distribution, i.e. the distribution of reorientational angles constrained to the interval $[0, \pi/2]$ since Θ and $\pi - \Theta$ cannot be distinguished for second-rank tensor interactions. This one-dimensional distribution with respect to the reorientational angle Θ is the maximum angular information one can obtain from a single 2D exchange spectrum of powder samples in the case of an axially symmetric spin interaction.

Both situations, sharp or broad featureless reorientational angle distributions (RADs) have, in fact been observed for chain motions in polymers. In the crystalline regions of semicrystalline polymers rotational motions occur around well-defined angles. This is demonstrated in Figure 8a, where a ^{2}H 2D exchange NMR spectrum of poly(vinylidene fluoride) (PVF_2) is shown.[57] This polymer is of particular interest because of its electrical properties.[58] The 2D spectrum for the crystalline α-phase at 370 K, in addition to a well-defined powder spectrum (Pake pattern) along the diagonal, displays elliptical exchange ridges. From this the RAD $P(\Theta)$ can be determined[59] and is plotted also. It exhibits two peaks, centered at $\Theta = 0°$ and $\Theta = 67°$. The latter indicates jump motions of the PVF_2 chains through the crystal lattice, which interchange C–^{2}H bond directions differing by $180° - 67° = 113°$, in agreement with the crystal structure.[58] Note that $P(\Theta)$ as shown in Figure 8a indicates an uncertainty of the reorientational angle of $\pm 3°$,[90] whereas the angular resolution of the 2D NMR experiment is as high as $\pm 1°$.[59] The broader RAD in PVF_2 therefore reflects the nonideal packing in a polymer crystal.

The geometry of the chain motion at the glass transition of amorphous polymers is not well-defined. This has been shown for polystyrene (PS) selectively deuterated at the polymer backbone (PS-d_3)[22,60] and for atactic polypropylene.[61] A full description of these studies has appeared elsewhere and for details the reader is referred to refs 22 and 61. A typical 2D exchange spectrum of PS-d_3 above the glass-transition temperature T_g is shown in Figure 8b. Here the spectrum along the diagonal is substantially broadened into the second frequency dimension. This broadening

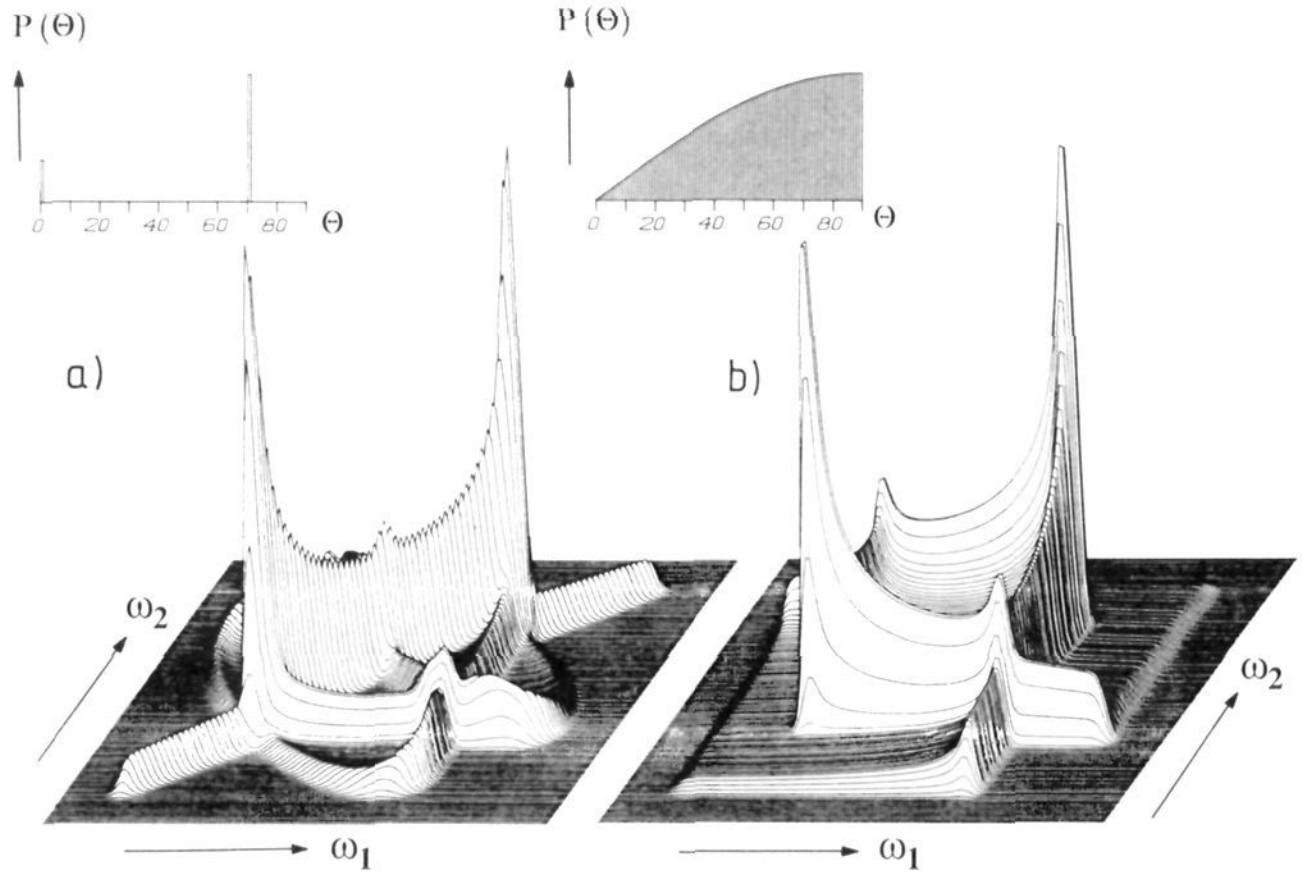

Figure 7. Simulated ^{2}H 2D spectra for different motional models in the limit of complete exchange ($t_m \gg \tau_c$): (a) chain motion on a diamond lattice (tetrahedral jumps) and (b) chain motion by isotropic rotational diffusion. The insets show the corresponding reorientational angle distributions $P(\Theta)$.

reflects relatively small frequency shifts during t_m caused by small angle rotations as shown in the RAD, P(Θ) extracted from the spectrum and displayed in Figure 8b. Moreover, significant exchange intensity extends over the entire 2D plane, but elliptical ridges are not observed. Large broad range frequency shifts during t_m translate into broad features in the RAD, where no specific angular region is favored. Such RADs result from isotropic rotational diffusion with a significant distribution of correlation times.[22,60] If the mean correlation times are extracted from temperature dependent 2D, solid-echo, and broad-line NMR experiments, the chain motion can be followed over a large dynamic range. The mean correlation times τ_c for the rotational motion of C–H bond directions follow the Williams–Landel–Ferry (WLF) equation[2] over 10 orders of magnitude with parameters in accord with those determined for the α-process from mechanical relaxation and light scattering.[60] This indicates a strong coupling of the motion of individual CH_2 groups to the cooperative motions responsible for the strong temperature dependence of the α-process in the vicinity of T_g.

Broad RADs apparently are characteristic of molecular motions at the glass transition of organic materials in general. Frozen liquid crystalline systems, however, differ from conventional organic glasses, because the mesogens are partially ordered. A particularly interesting partially ordered glass has recently been obtained from a columnar liquid crystal formed by a chiral discotic mesogen.[62] By combining ^{2}H NMR and broadband dielectric spectroscopy the glass transition can be related directly to the axial motion of the disks around the column axis. Its dynamics follows the WLF equation with parameters very similar to those of other organic glasses. Of particular interest then is the geometry of that axial motion. The pseudo-3-fold symmetry of the discotic (Figure 8c) suggests rotations by 120°, whereas diffusive motions would allow all reorientational angles from 0 to 360: The 2D spectrum shown in Figure 8c displays exchange intensity confined within elliptical figures, but the elliptical ridges themselves are largely washed out due to the uncertainty of the reorientational angle corresponding to a RAD which peaks at 60° = 180° − 120° but which has a width of as much as ±15°. Two-dimensional exchange NMR thus allows us to determine quantitatively the partial confinement of the axial motion in a frozen liquid crystalline system.

As mentioned above, 2D exchange NMR is not limited to deuterons. It can likewise be applied, for example, to natural abundance ^{13}C. Moreover the information about the geometry of the motion is even higher, if partially ordered samples are available. As an example, Figure 9 shows experimental and calculated ^{13}C 2D exchange spectra of highly oriented poly(oxymethylene) (POM) at 360 K, taken from ref 23. The characteristic off-diagonal exchange patterns are readily analyzed as resulting from the helical jump motion[63] of this semicrystalline polymer. For the 9_5 helix the elementary process involves a rotation of ±200°. The ridge for ±200° extends essentially perpendicular to the diagonal, and shows up in the contour plots "like the wings of an airplane". The ridge for ±400° rotations looks like an ellipse with its long axis along the diagonal. These two prominent ridges are clearly visible in Figure 9. Even the much weaker one for ±600°, extending far into the 2D plane has been located.[23] The correlation times determined from various ^{13}C exchange NMR experiments in the temperature range 300–370 K show an Arrhenius behavior with an activation energy E_A = 75 ± 8 kJ in good agreement with mechanical and dielectric data for the α-relaxation of this polymer.[23]

Two dimensional exchange NMR can also be applied to study the molecular dynamics of additives to polymer glasses. This has recently been demonstrated by Jones and co-workers,[64] who reported 2D spectra of a phosphate ester diluent in a blend of polystyrene and

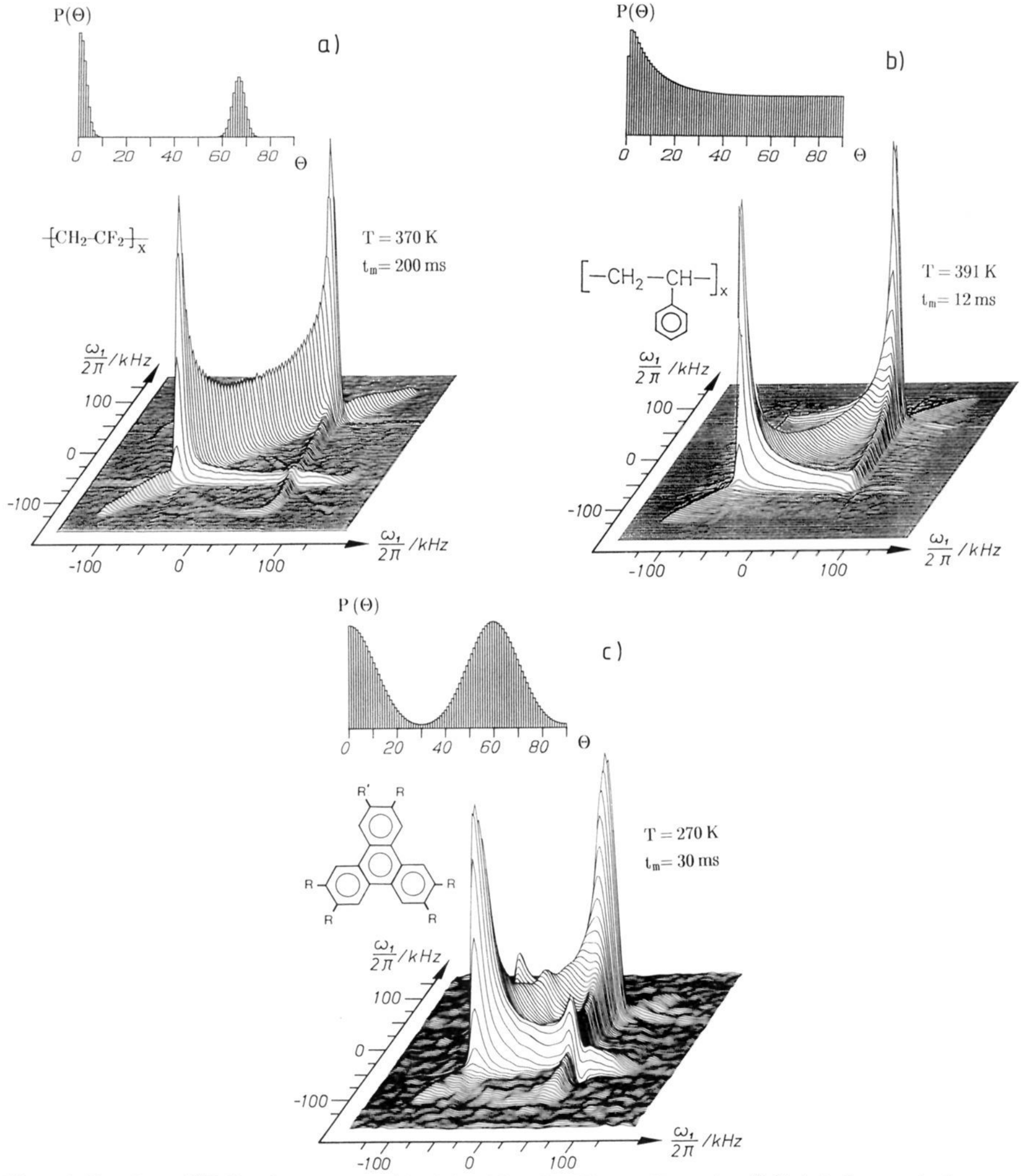

Figure 8. Experimental ^2H 2D exchange spectra: (a) poly(vinylidene fluoride) crystalline α-phase,[57] (b) chain deuterated polystyrene above its glass transition,[22] and (c) columnar liquid crystal based on a triphenylene core above its glass transition,[62] (R = OC_5H_{11}, R_1 = $OCOCHClCHCH_3C_2H_5$). The insets show the RADs derived from the analysis of the 2D spectra.

poly(phenylene oxide). They show that the diluent commences diffusional motion at the same temperature as the loss peak in the mechanical relaxation spectrum is detected.

Last but not least, we would like to mention that 2D exchange spectra completely analogous to the ones discussed here in terms of molecular dynamics can also arise from spin diffusion[20] among, for example, ^{13}C nuclei residing on neighboring molecules within polymeric solids. The exchange patterns then provide the relative orientation of the corresponding shift tensors and, therefore, structural information. Applications of this technique will be discussed in section VI.C below.

B. Extension to 3D Exchange NMR

For complex motions even the information accessible by 2D techniques is not sufficient for an adequate de-

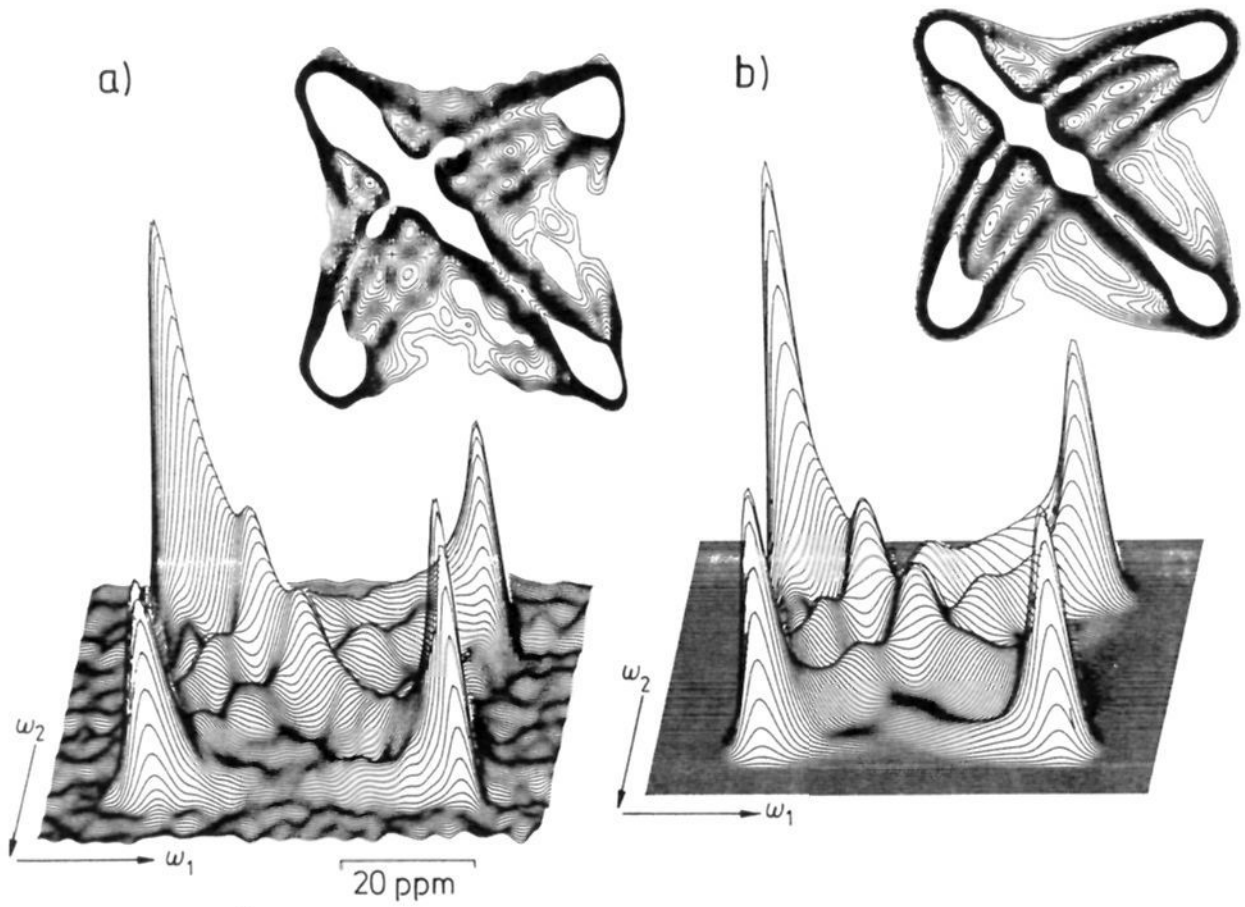

Figure 9. ^{13}C 2D exchange spectrum[23] of highly oriented poly(oxymethylene) at $T = 360$ K, $t_m = 2$ s. The angle between the director axis and B_0 is $\beta_0 = 45°$.

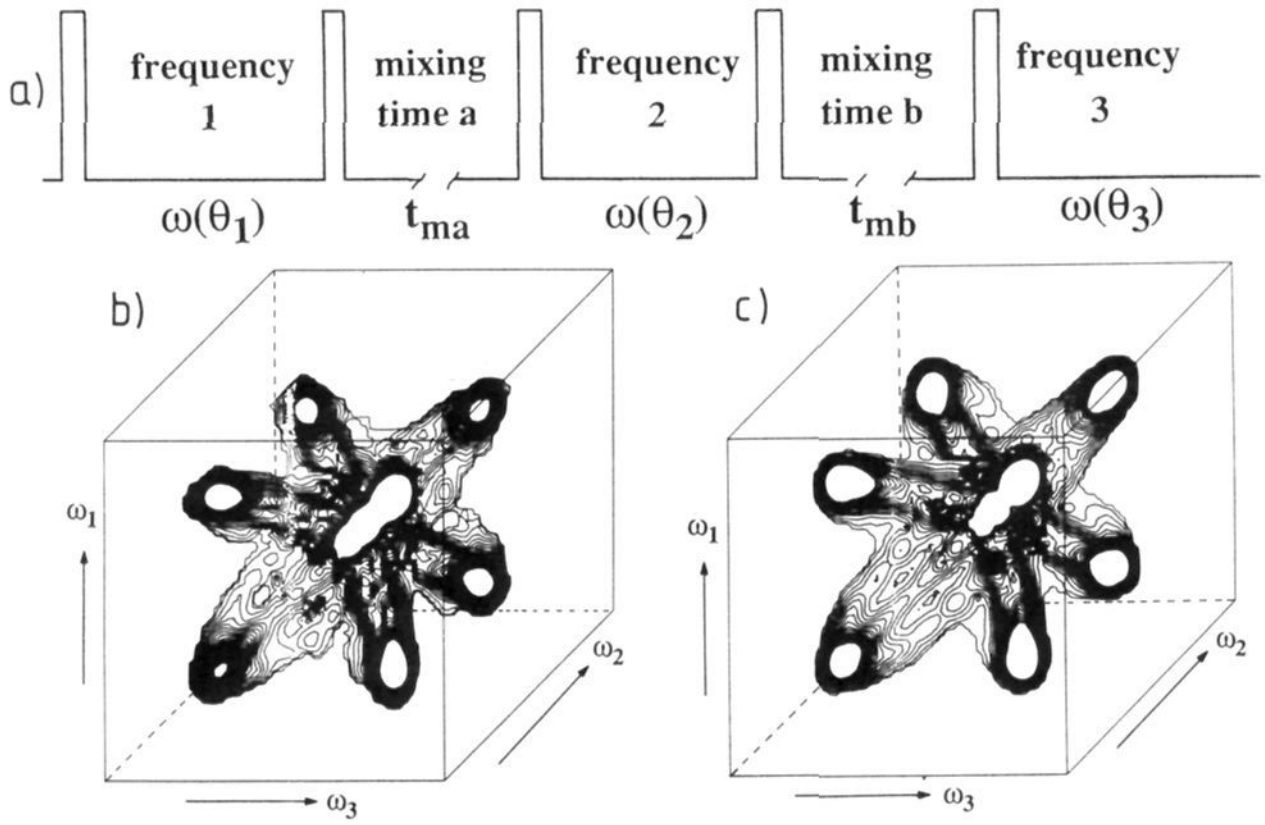

Figure 10. ^{13}C 3D exchange spectrum[65] of highly oriented polyoxymethylene (cf. Figure 9): (a) pulse sequence, (b) experimental spectrum $t_{ma} = t_{mb} = 1$ s (all other conditions as for Figure 9), and (c) simulated spectrum.

scription of the motional mechanisms involved. This is partly due to a lack of spectral resolution, as observed for example, overlap of exchange intensity for different carbon positions in a monomer unit. The deficiency of 2D NMR for characterizing motional *mechanisms*, however, is more fundamental. Since in 2D NMR we measure the orientation of molecules only *twice*, there is no information about the trajectory a molecule follows when rotating from one orientation to another. In order to distinguish different mechanisms one has to determine the molecular orientation at least *three* times. Therefore three-dimensional exchange NMR has been introduced recently.[65]

As shown in Figure 10a, after a first evolution time t_1 we introduce a first mixing time t_{ma}, followed by a second evolution time t_2 and a second mixing time t_{mb}. The data are finally acquired during the detection time t_3. Three subsequent FTs, over t_1, t_2, and t_3 yield the intensity as a function of three frequencies ω_1, ω_2, and ω_3, respectively, as shown in Figure 10, parts b and c, for the highly ordered POM sample discussed above.[63] The helical jump motion of this polymer leads to characteristic exchange ridges throughout the 3D cube. The total measuring time was 24 h, proving that 3D NMR in solids is indeed feasible.

In the 3D spectrum the different *pathways* persued by the molecules from the first evolution time to the detection time lead to *different* exchange signals and can, therefore, be distinguished. In POM, for example, a total rotation by +200° can be achieved via a single step or by two subsequent rotations to reach +400° during t_{ma} followed by a backrotation −200° during t_{mb}.

The quantitative analysis[65] of the data in Figure 10 shows that the helical jump motion always occurs by the elementary process, i.e. rotation by ±200°. Thus a ±400° rotation occurs by two rotations in the same direction.

We stress again that multidimensional exchange NMR provides information that is *not* available from 2D exchange experiments, even if they are performed for different mixing times. Therefore they give new insight into the complex motions of amorphous polymers at the glass transition. This has recently been demonstrated for poly(vinylacetate) where reduced 4D exchange NMR revealed the nature of the nonexponential relaxation above T_g.[66]

C. Rotating Samples (MAS)

Two dimensional exchange NMR not only can detect molecular dynamics via the resulting rotations of individual groups of the monomer unit, but as demonstrated recently,[67] it is also able to detect chain diffusion from crystalline to amorphous regions in semicrystalline polymers. Although occasionally postulated this process has not been accepted as a general concept, most likely because of lack of experimental evidence.

Our 2D experiment makes use of the fact that under MAS the all-trans conformation in the crystalline regions of polyethylene (PE) has an isotropic chemical shift that differs by approximately 2 ppm from that of the gauche-containing conformers in the amorphous regions. In the sketch of PE chains in a crystallite near the interface to an amorphous region shown in Figure 11a carbons 1 and 2 would contribute to the "amorphous" signal (marked a in Figure 11b) and the carbons 9 and 10 would contribute to the "crystalline signal" (marked c). The exchange intensity between the ^{13}C signals for CH_2 groups in the crystalline and in the amorphous regions is clearly visible in Figure 11b. This directly proves chain diffusion taking CH_2 groups from the crystalline into the amorphous regions and vice versa. This translational diffusion in the solid state results from the well-known α-process, assigned to 180° jumps of the chain stems in the crystallites[68] accompanied by a translation by one CH_2 unit. The quantitative analysis of our 2D NMR and relaxation data[67] yields jump rates in complete agreement with previously reported values (activation energy E_a = 105 kJ/mol). It shows that the rms displacement of individual CH_2 groups amounts to more than 100 nm within 100 s near 360 K corresponding to a translational diffusion constant of 10^{-14} cm^2/s.

Whereas in the latter example 2D exchange spectra were recorded with relatively high spinning speeds ($\omega_R = 2\pi \times 4$ kHz) such that centerbands only are observed, 2D MAS-NMR can also be used to study slow rotational motions. To this end the spinning speed must be reduced to generate a significant number of sidebands. Then the basic pulse sequence for 2D exchange NMR, described above (Figure 6), can be applied. As shown in Figure 12a the rf pulses have, however, to be synchronized with the rotor. Instead of exchange ridges resulting from molecular dynamics in static samples, 2D exchange *sideband* patterns are observed for long mixing times as depicted in Figure 12b.

The two-dimensional MAS exchange experiment that makes use of such sideband patterns was first demonstrated by Veeman et al.[24,63] They recorded absolute mode spectra only. This must be considered a major drawback, since *pure absorptive* spectra are much better resolved. An advanced version of the 2D MAS exchange experiment involving four data sets has been designed by Hagemeyer et al.[23] It permits purely absorptive 2D sideband patterns to be recorded under MAS. As usual sine or cosine components are selected by adjusting the relative phases of cross polarization and the $\pi/2$ pulse at the end of the evolution time (Figure 12a). In two of the four experiments the mixing time t_m is set to an integer multiple of the rotor period T_R, $t_m = nT_R$. In the other two experiments time-reversal in t_1, through $t_m = nT_R - t_1$, is achieved by adjusting the time interval from the end of the cross-polarization to the $\pi/2$ pulse terminating the mixing time to nT_R. As described in detail in ref 23, the four data sets can then be combined to yield absorptive 2D spectra.

Another example of a 2D exchange technique is due to Harbison et al.[69] combining 2D exchange with chemical shift scaling.[38] This method is particularly useful for motions that occur between sites which can be distinguished by their isotropic chemical shift.

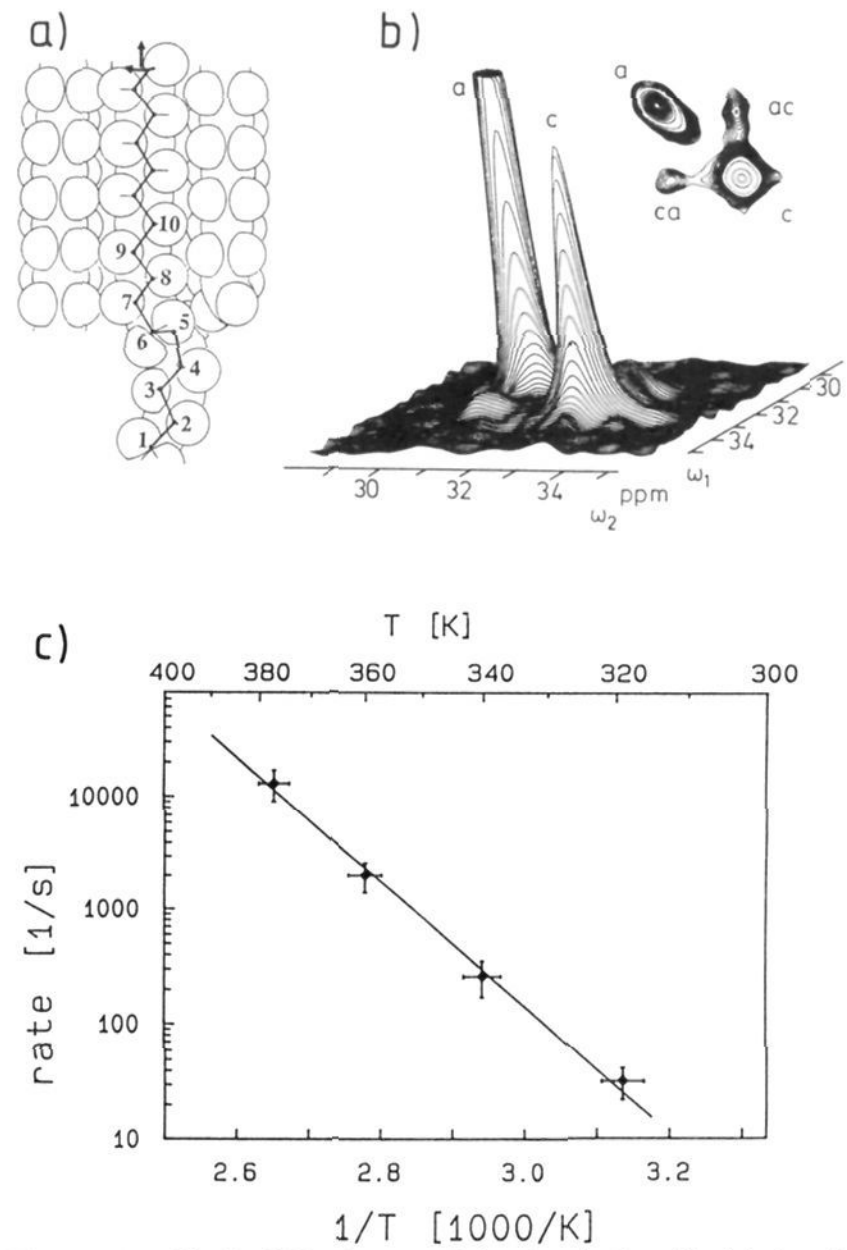

Figure 11. Chain diffusion in solid polyethylene:[67] (a) sketch of polyethylene chains in a crystallite, near the interface to an amorphous region (the repeat units of one chain extending into the amorphous region are marked by numbers), (b) ^{13}C 2D MAS spectrum at T = 363 K, signal of the crystalline regions suppressed by single pulse excitation with a recycle delay of 4 s (in the stack plot, the amorphous peak was cut at 25% of its maximum; since isotropic chemical shifts only are detected rotor synchronization is not needed in this case), and (c) Arrhenius plot of jump rates for the primary step of chain diffusion in polyethylene.

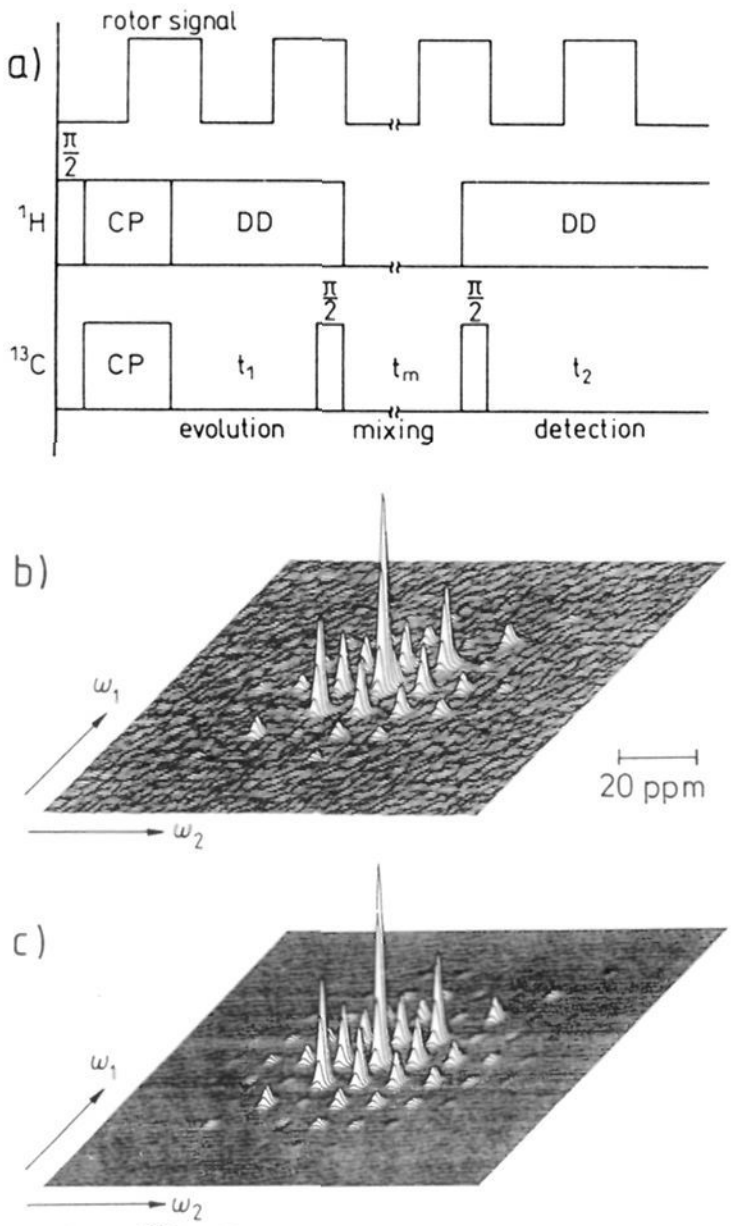

Figure 12. ^{13}C 2D MAS exchange spectra of poly(oxymethylene):[23] (a) pulse sequence synchronized with the rotor, (b) experimental spectrum (T = 360 K, t_m = 2 s, spinning speed $\omega_R = 2\pi \times 750$ Hz), and (c) calculated sideband pattern.

V. Rotor-Synchronized MAS-NMR of Partially Ordered Polymers

A. Determination of Orientational Distribution Functions

Solid-state NMR has also opened up new possibilities for a detailed characterization of molecular order in polymers. The selectivity of NMR allows one to ascertain preferential orientation of several functional groups in the monomer unit. Thus overall alignment of the polymer chain can be distinguished from conformational order. Moreover, the complete orientational distribution function (ODF) in amorphous polymers can be determined by solid-state NMR, whereas other spectroscopic techniques yield low moments only of this function, i.e. the second moment (IR dichroism, refractive index) or second moment and fourth moments (fluorescence and Raman band-shape analysis).

It has been realized only relatively recently,[26] that 2D MAS-NMR can also be used in this area. This is attractive because the increased spectral resolution offers a means to study the orientation of several functional groups simultaneously. If an ordered sample is spun with the order axis not parallel to the rotor axis, phase and intensity modulations of the centerbands and sidebands are observed which depend on the point in time the spins begin their evolution, e.g. the FID, after being excited.[26] Therefore, new signals are introduced

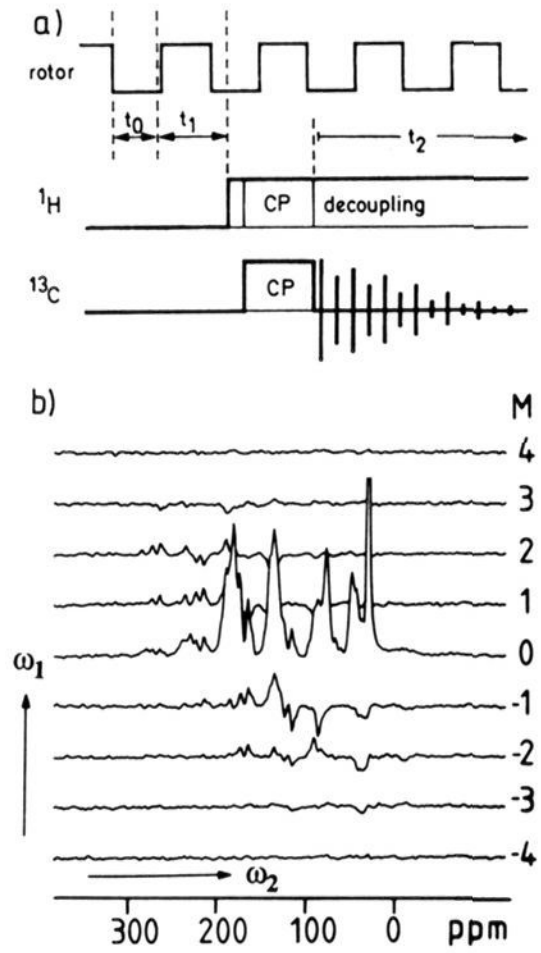

Figure 13. Rotor-synchronized ^{13}C 2D MAS-NMR for determination of the orientational distribution function:[26] (a) Pulse sequence (the offset t_0 is adjusted in order to phase the spectrum in ω_1) and (b) experimental spectrum[70] of a commercial high modulus fiber composed of HBA and HNA (Hoechst-Celanese). The angle between the director axis and B_0 is $\beta_0 = 60°$, spinning speed $\omega_R = 2\pi \times 3.7$ kHz. The chemical shift scale refers to TMS.

by synchronization of the data acquisition with the rotor position Ψ, cf. Figure 13a and eq 3. For each resonance a sideband pattern in two dimensions can be obtained, simply by taking the rotor position as the evolution period t_1 and observing the MAS FID during the subsequent detection period t_2. Because of the rigorously cyclic, nondecaying behavior of the experiment during t_1, it is completely sufficient to sample over a single rotor period T_R in at most 16 steps. The corresponding 16 slices of the 2D FT, spaced by ω_R in ω_1, contain all the information available from the experiment.

Figure 13b illustrates the technique with a commercial high modulus fiber (Hoechst-Celanese), based on a liquid crystalline copolymer of hydroxy benzoic acid (HBA, 73%) and hydroxynaphthalene (HNA, 27%). If the fiber were completely disordered, sidebands would be restricted to the M = 0 center slice. Sideband intensities are clearly detected, however, from $M = -3$ to $M = +3$, indicating a high degree of orientation.[70]

The quantitative analysis of 2D MAS spectra requires efficient numerical tools. The basis of the method developed to this end[26] will, therefore, briefly be outlined. For simplicity, only uniaxially ordered samples will be considered, where the order can be characterized by a one-dimensional ODF $P(\chi)$, where χ denotes the angle between a molecular frame of reference, typically a local chain direction, and the macroscopic order axis. Then the ODF can conveniently be expanded into a series of Legendre polynomials $P_l(\cos \chi)$:

$$P(\chi) = \sum_l \frac{2l+1}{8\pi^2} \langle P_l \rangle P_l(\cos \chi) \qquad (13)$$

where the sum runs over all even values of l. The averages $\langle P_l \rangle \equiv \langle P_l(\cos \chi) \rangle$ are the moments of the ODF and are all in the range $0 \leq \langle P_l \rangle \leq 1$, where the ex-

tremes correspond to an isotropic sample (no order) and a completely aligned sample (full order).

As shown in ref 26 the 2D MAS-NMR spectrum $S(\omega_1, \omega_2)$ can then likewise be expanded into a series of 2D subspectra $S_l(\omega_1, \omega_2)$, from which the moments of the ODF are directly obtained via

$$S(\omega_1, \omega_2) = \sum_l \frac{2l+1}{8\pi^2} \langle P_l \rangle S_l(\omega_1, \omega_2) \qquad (14)$$

The subspectra $S_l(\omega_1, \omega_2)$ must be calculated only once for each respective ^{13}C position. They depend on the shielding tensor, the rotor frequency ω_R, and the orientation of the sample in the rotor. The subsequent data-fitting procedure for determination of $\langle P_l \rangle$ is straightforward. For the example of Figure 13b higher moments $\langle P_l \rangle$ with $l > 2$ are significant (see also ref 70).

B. 3D ^{13}C MAS-NMR: Correlation of Molecular Structure, Order, and Dynamics

In heterogeneous solids, e.g. semicrystalline or glassy polymers, the time scale or even the mechanism of molecular motions may depend on the degree of order. Therefore, experiments are desirable, which can *correlate* these two properties. In order to achieve this goal a 2D experiment combining exchange NMR and rotor-synchronized MAS techniques with rotations in spin space by TOSS (cf. section III.B) has been designed.[71] Better resolution and a significant gain in information content concerning both order and dynamics, can be achieved, however, by extending the experiment to a *third* frequency dimension.[72]

To this end the 2D experiments described above for monitoring molecular dynamics and for detecting molecular order have been combined to produce a rotor-synchronized 3D experiment which correlates these two phenomena. Besides achieving this correlation, the CORD (correlation of order and dynamic) 3D experiment[72] also is important for providing information about the geometry of dynamic processes. As noted in ref 23 2D-MAS exchange sideband patterns contain rather limited information only about the geometry of molecular motions. In partially ordered samples it should be possible to discriminate more easily between different geometries. As will become apparent below, the off-center planes of the 3D spectra provide this information.

The pulse sequence for the rotor-synchronized 3D MAS experiment is shown in the upper part of Figure 14. As in the 2D experiment for detection of molecular order, the pulse programmer is started by the rotor signal. Then an evolution time t_1 is inserted and subsequently incremented in typically eight steps $\Delta t_1 = T_R/8$, where T_R is the rotor period. At the end of t_1 a proton $\pi/2$ pulse is executed followed by cross-polarization (CP). Rather than recording the ^{13}C signal thereafter, CP is followed by a 2D exchange sequence[20] with a second evolution time t_2, a mixing time t_m, and a detection time t_3, during which the ^{13}C signal is acquired. In order to generate pure absorptive spectra four data sets are recorded, where the mixing time is pairwise $t_m = nT_R$ or $t_m = nT_R - t_2$, respectively, with properly adjusted rotor phase.

Depending on whether or not the sample is ordered and dynamic processes occur that change the NMR frequency during t_m, different 3D sideband patterns are

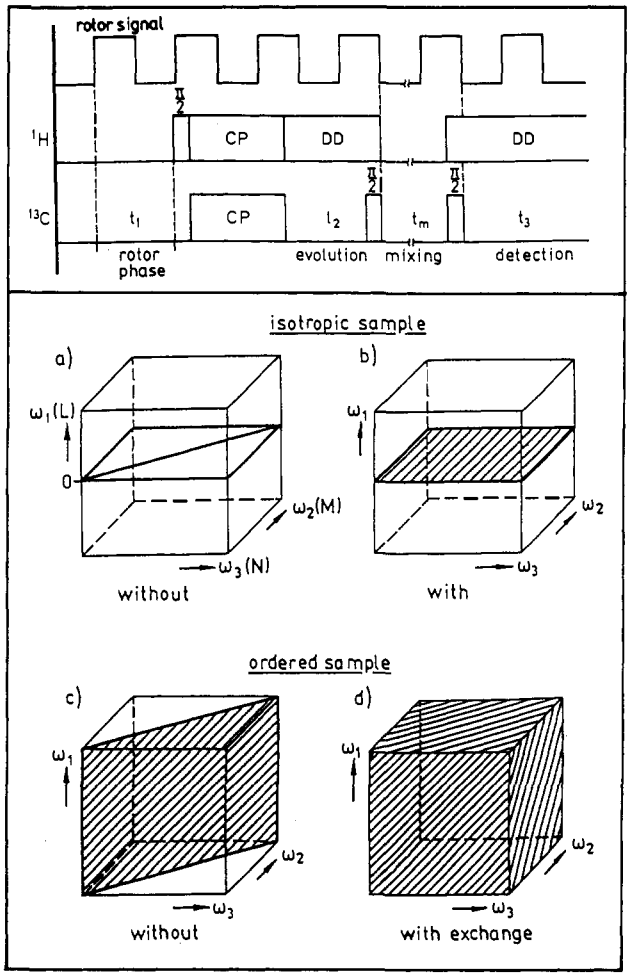

Figure 14. ^{13}C 3D MAS-NMR correlating molecular structure, order and dynamics.[72] The top section shows the pulse sequence of the rotor-synchronized 3D CORD experiment. The bottom section shows the schematic representation of the general features of 3D CORD spectra: (a) powder sample without exchange, (b) powder sample with exchange, (c) ordered sample without exchange, and (d) ordered sample with exchange. The orders of the sidebands in ω_1, ω_2, and ω_3 are labeled by integers L, M, and N, respectively.

expected as depicted schematically in Figure 14. Consider an isotropic sample first, then the total NMR signal is not modulated during t_1 and the sideband pattern is confined to the horizontal plane $\omega_1 = 0$, Figure 14b. In absence of exchange (short $t_m \approx T_R$) the spectrum even becomes diagonal (Figure 14a). For an *ordered sample*, however, in which no dynamic processes occur which interchange NMR frequencies during t_m, the sideband signals are confined to the cross-diagonal plane $\omega_2 = \omega_3$ (Figure 14c). This 2D spectrum thus resembles the rotor-synchronized spectra[26] discussed above. It contains the information about the structure as revealed by the chemical shift. Therefore we refer to this plane as the structure and order plane.

Signals in the full 3D cube (Figure 14d) result only if frequency exchange due to a dynamic process occurs during t_m. Sidebands off the planes marked in Figure 14, part b and c, can occur only if the residue giving rise to the NMR signal is involved in *both* the order *and* the dynamics. Such off-plane sidebands, therefore, *correlate* these two properties and provide valuable geometric information about the dynamic process under study. Here, only molecular motions will be considered explicitly as a source of dynamic processes. It is im-

portant to point out, however, that the 3D CORD experiment can likewise be applied to study the correlation between molecular order and spin diffusion,[20,27,71] which may be enhanced by proper choice of the rotor frequency.[73] In this way the 3D CORD experiment offers a means to exploit partially ordered samples for obtaining improved structural information under high spectral resolution.

The first 3D CORD spectra were recorded for a sample of highly oriented POM poly(oxymethylene) and are displayed in Figure 15. The spectrum at the left was recorded at T = 300 K with a mixing time of only t_m = 2 ms. Clearly all the sidebands are confined to the "structure and order plane" $\omega_2 = \omega_3$ defined above, since under those conditions exchange of NMR frequencies due to the helical jump motion cannot occur. Both positive and negative sidebands, however, extend up to the third order in ω_1, showing the high molecular order of the sample. The spectrum on the right (Figure 15), on the other hand, recorded at 360 K and a mixing time as long as t_m = 1.5s, displays a large number of positive and negative off-diagonal sidebands, indicating molecular motion on this time scale. As shown in detail in ref 72 these sideband patterns can quantitatively be analyzed in terms of the helical jump motion of the POM 9_5 helix. The off-diagonal exchange induced sidebands have high intensities, due to the strong correlation between order and motion, since the helix axis is the order axis, as well as the axis around which the molecular motion occurs. Since pure absorptive sidebands with both positive and negative intensities are recorded in the whole 3D cube, the spectrum is sensitive to the details of the motional mechanism.

The possibility of generating a complete new frequency dimension by just sampling the rotor period by eight or at most 16 steps opens up numerous ways of generating 3D MAS spectra of partially ordered solids. A particularly important one has recently been realized in our laboratory, where the three frequency-dimensions probe respectively the isotropic, isotropic as well as anisotropic chemical shift, and molecular order. The advantage of that experiment is, that 2D planes taken from the 3D cube display 2D sideband patterns for each carbon position separately with a spectral resolution equal to that in a high speed spinning spectrum without sidebands. The time necessary for data accumulation is not more than that required for a static 2D experiment. It can, therefore, be anticipated that the information about anisotropic interactions contained in sideband patterns can be fully exploited in 3D solid-state NMR.

VI. Spin Diffusion: Morphology, Phase Separation, and Miscibility in Multicomponent Polymers

Solid-state NMR is also a powerful tool for the analysis of the microstructure in semicrystalline polymers, block copolymers, and polymer blends. The proximity of monomer units is probed via spin diffusion,[27] i.e. the diffusion of nuclear magnetization through the polymer without transport of material. It is affected via mutual flips of dipole–dipole coupled nuclei. Spin diffusion, therefore, is most effective for abundant nuclei with high magnetic moments, in particular ^{1}H. For short times the mean-square distance $\langle x^2 \rangle$ the magnetization moves within time t is given by $\langle x^2 \rangle = aDt$, where D is the spin diffusion constant. The prefactor a depends on the geometry of the packing, e.g., lamellar, cylindrical, or spherical, and D is related to the strength of the dipolar coupling as reflected in the width of the ^{1}H NMR spectrum. The various spin diffusion techniques can probe chemical or physical heterogeneities in polymers on a length scale between approximately 1 and 100 nm and therefore, provide important information complementary to that obtained from the various techniques of electron microscopy which are particularly suited for detecting structures above approximately 20 nm.[74]

A. Proton Spin Diffusion with ^{1}H Detection

This has been used extensively in the past to study the morphology of semicrystalline polymers. For a recent review of such studies on polyolefins see ref 75. Pulsed experiments have been designed which can separate broad and narrow components in the ^{1}H NMR spectrum resulting from different chain mobilities in the crystalline and amorphous regions. Their drawback, however, is the lack of spectral resolution in solid-state ^{1}H NMR. Multiple-pulse homonuclear decoupling eliminates the major source of line broadening. Applying multiple-pulse sequences during the preparation of selective proton magnetization and during the detection period enhances the resolution,[28,76,77] which can further be improved by combination with MAS (CRAMPS).

The most advanced approach is due to Ernst et al.[78] applying CRAMPS in combination with 2D exchange NMR.[20] In the model polymer blend polystyrene (PS)/poly(vinyl methyl ether) (PVME), which can be prepared as a homogeneous or as a heterogeneous mixture, the mixing of the two polymers on a molecular level in the former was proven via a cross-peak between the O–CH_3, O–CH signals of PVME and the aromatic proton signals of PS. This cross-peak was absent in the heterogeneous mixture. For measurements of the spin-diffusion coefficient as well as the composition of the mixed phase, however, 1D selective inversion–recovery and saturation–transfer experiments under CRAMPS conditions combined with spin diffusion proved to be better suited.[29]

B. Spin Diffusion with ^{13}C Detection

The spectral resolution of solid-state ^{1}H NMR even with CRAMPS is not high enough to unravel the signals of the different components in complex mixtures. Therefore, techniques have been developed which exploit the higher resolution of ^{13}C MAS-NMR. Most of these experiments, however, are difficult to analyze quantitatively, since selection of proton magnetization is based upon relaxation parameters such as T_1, $T_{1\rho}$, and T_2. Nevertheless, these techniques have proven useful in providing information about the interface between crystalline and amorphous regions, e.g., in polyethylene.[79-81] Even more importantly they have been successfully applied to study domain sizes, composition, and internal surface effects in various polymer blends and block copolymers.[12,82-88]

The superior spectral resolution of ^{13}C NMR can likewise be exploited in ^{13}C–^{13}C spin diffusion studies. Due to the low natural abundance of ^{13}C, spin diffusion

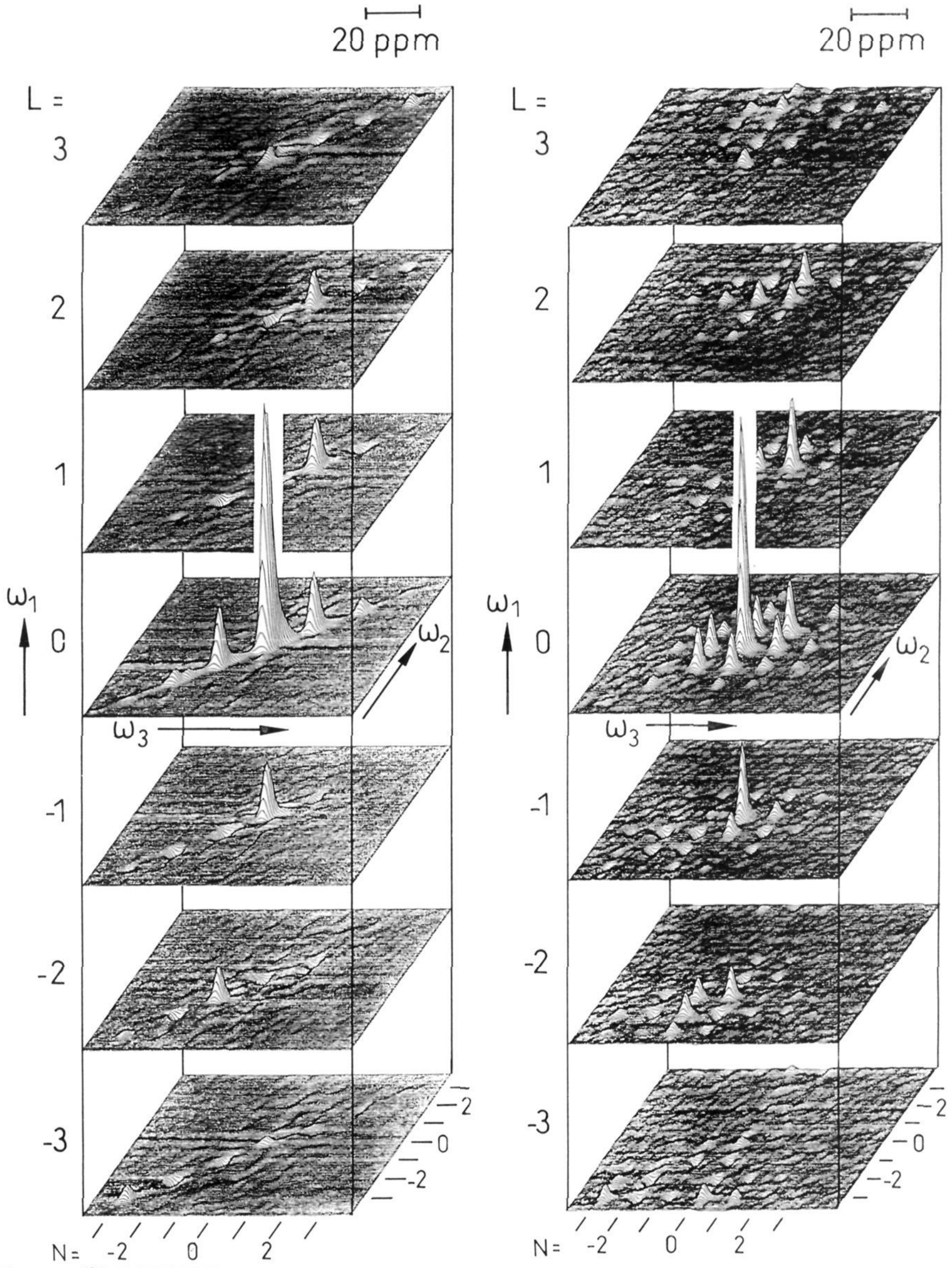

Figure 15. ^{13}C 3D MAS-NMR spectra of highly oriented poly(oxymethylene): (left) T = 300 K, t_m = 2 ms; and (right) T = 360 K, t_m = 1.5 s, (adopted from ref 72).

constants of carbons are typically at least 100 times smaller than those of protons. The inefficiency of ^{13}C–^{13}C spin diffusion can be overcome by ^{13}C isotopic labeling, as demonstrated, for example, on blends of poly(ethylene terephthalate) and polycarbonate.[87,88] Spin diffusion between ^{13}C in natural abundance can,

however, be substantially accelerated by adjusting the rotor frequency in MAS to an integer fraction of the isotropic chemical shift difference between two particular carbon resonances. This provides a coupling between spin flip processes and mechanical rotation of the sample.[73,89] In principle, this technique can provide high selectivity because the spin diffusion rate between selected carbon positions can be driven separately.

Recently, novel schemes for selection of proton magnetization, proton spin diffusion and high-resolution ^{13}C MAS detection have been developed.[31] The proton magnetization selection is achieved under CRAMPS. In heterogeneous systems with significant differences in molecular mobility, e.g., semicrystalline polymers or block copolymers involving glassy and rubbery components, a dipolar filter pulse sequence is applied, which exploits differences in the dipole–dipole coupling. Spin diffusion is then allowed to take place, followed by detection after cross-polarization to ^{13}C. This technique has not only demonstrated the existence of interfacial zones between crystalline and noncrystalline regions in polyethylene,[70b,90] but allowed evaluation of their thickness (1.2 ± 0.5 nm) in both high-density Lupolen 5260 z and low density Dowlex 2045 E. Moreover, the highly resolved ^{13}C NMR spectra showed that the chains in the interfacial regions are conformationally disordered similar to those in the noncrystalline regions but are restricted in mobility due to their proximity to the crystallites.

In rigid systems a chemical shift filter pulse sequence can be applied prior to the spin diffusion period to differentiate, for example, aliphatic from aromatic protons, etc. As a particularly clear-cut case this technique has been applied to a series of symmetric diblock copolymers of PS and poly(methyl methacrylate) (PMMA).[91] In Figure 16 the increase of the carbon signals of the phenyl ring in the PS block after selection of the PMMA block is plotted against the spin diffusion time for various block lengths. The equal lengths of both blocks in the symmetric copolymers ensures a lamellar structure which makes the quantitative analysis of the data easy. PMMA and PS are known to be immiscible. The spin diffusion data yield domain sizes which are consistent with the scaling law $M_n^{0.66}$ where M_n denotes the molar mass of the blocks, as predicted theoretically.[92] For comparison, a statistical copolymer, in which no phase separation is possible and a blend of both homopolymers were included in the data set. The close agreement between experimental intensities and the time dependence calculated from the diffusion equation is apparent in Figure 16b and demonstrates that domain sizes between 0.5 and 100 nm can be determined quantitatively. This technique has already been applied to a number of homogeneous and heterogeneous polymer systems, in particular to a miscible blend of two high performance polymers, an aromatic poly(ether imide) and a poly(aryl ether ketone).[31]

C. Structural Studies from ^{13}C Spin Diffusion

As mentioned above in section IV.A, 2D exchange NMR spectra governed by spin diffusion allow the determination of the relative orientations of nearby molecules in polycrystalline and noncrystalline solids. This was demonstrated by Henrichs et al. on ^{13}C-labeled

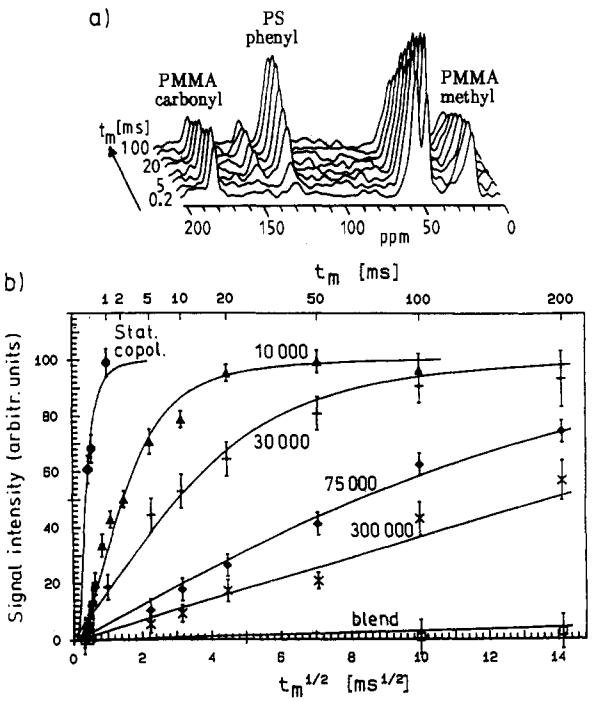

Figure 16. Spin diffusion as a tool to determine domain sizes in heterogeneous polymers:[31] (a) ^{13}C MAS spectra of the symmetric diblock copolymer PS-b-PMMA[91] (M_n = 30.000 g/mol) as a function of the diffusion time t_m (the intensities of the spectra are scaled to that of the methyl signal in PMMA) and (b) signal intensity of the phenyl carbons in PS as function of t_m (the solid lines are fits to the data based on the diffusion equation with a spin diffusion constant D = 0.6 nm^2/ms; the lamella thickness increases from d = 4.5 nm for M_n = 10.000 g/mol to d = 60 nm for M_n = 300.000 g/mol).

zinc acetate dihydrate[93] and has recently been taken up by Tycko et al.[94] With appropriate isotopic labeling 2D exchange NMR may be used to determine the relative orientations of different functional groups on the same molecule or polymer chain, i.e. molecular conformation. Moreover, this technique can probe the packing of the monomer units in amorphous polymers and check to what extent neighboring units pack uniformly.

Under conditions of MAS spin diffusion between ^{13}C can be enhanced by rotational resonance.[89,95] This then allows the measurement of internuclear distances between sites separated by as much as 0.5 nm as demonstrated recently by Griffin et al.[96]

VII. Conclusions

High-resolution NMR in liquids is an indispensable analytical tool for structural characterization in chemistry. Particularly in biochemistry, the necessary spectral resolution can only be achieved, however, by two-dimensional and higher dimensional spectroscopy. An analogous situation is encountered in solid polymers. Unless isotopic labeling is employed the different anisotropic spin interactions can be separated only via two- and three-dimensional techniques. Besides providing structural information, multidimensional solid-state NMR offers unique possibilities for characterizing slow molecular dynamics and relating it to macroscopic material behavior.

Development of new experimental methods is far from complete. In fact, some of the experimental examples presented here, in particular in ^{13}C NMR, only demonstrate the feasibility of the new techniques.

Eventually, one would like to have the various kinds of information dealt with here not only for the bulk sample but also with spatial selectivity. Therefore, NMR imaging techniques are being developed in a number of laboratories (for a recent review see ref 97). In fact, the first spatially resolved wide-line ^2H NMR spectra of solid polymers, which contain information about molecular order and dynamics have already been recorded,[98] by employing 2D Fourier imaging with double quantum evolution. It can be anticipated, therefore, that the importance of multidimensional solid-state NMR in polymer science will substantially increase in the future.

Acknowledgments. It is a pleasure to thank my coworkers engaged in much of the work, described here: Drs. B. Blümich, J. Clauss, A. Hagemeyer, J. Hirschinger, S. Kaufmann, J. Leisen, D. Schaefer, K. Schmidt-Rohr, Y. Yang, and K. Zemke. Financial support by the Deutsche Forschungsgemeinschaft (Leibniz-program, SFB 262) and the Bundesministerium für Forschung und Technologie is highly appreciated and gratefully acknowledged. Special thanks are also due to Drs. B. Chmelka and J. Titman for carefully checking the manuscript.

References

(1) McCrum, N. G.; Read, B. E.; Williams, G. *Anelestic and Dielectric Effects in Polymer Solids*; John Wiley: New York, 1967.
(2) Ferry, J. D. *Viscoelastic Properties of Polymers*; John Wiley: New York, 1980.
(3) Ward, I. M *Mechanical Properties of Solid Polymers*; John Wiley: New York, 1971.
(4) Ward, I. M., Ed.; *Structure and Properties of Oriented Polymers*; Applied Science Pub.: London 1975.
(5) (a) Bailey, R. T.; North, A. M.; Pethrick, R. A. *Molecular Motions in High Polymers*; Clarendon Press: Oxford, 1981. (b) Hedvig, P. *Dielectric Spectroscopy of Polymers*; Adam Hilger: Bristol, 1977.
(6) Bovey, F. A. *Nuclear Magnetic Resonance Spectroscopy*, 2nd ed.; Academic Press: New York, 1987.
(7) Komoroski, R. A., Ed. *High Resolution NMR Spectroscopy of Synthetic Polymers in Bulk*; VCH Publishes: New York, 1986.
(8) Schaefer, J.; Stejskal, E. O. *J. Am. Chem. Soc.* **1976**, *98*, 1031.
(9) Mehring, M. *High Resolution NMR in Solids*, 2nd ed.; Springer: Berlin, 1983.
(10) Fyfe, C. A. *Solid State NMR for Chemists*; CFC Press: Guelph, 1983.
(11) Veeman, W. S. *Progr. NMR Spectroscp.* **1984**, *16*, 193.
(12) Voelkel, R. *Angew. Chem., Int. Ed. Engl.* **1988**, *27*, 1468.
(13) Tonelli, A. E. *NMR Spectroscopy and Polymer Microstructure: The Conformational Connection*; VCH: New York, 1989.
(14) Jelinski, L. W. *Anal. Chem.* **1990**, *62*, 212R.
(15) Spiess, H. W. *Annu. Rev. Mat. Sci.* **1991**, *21*, 131.
(16) Spiess, H. W. *Adv. Polym. Sci.* **1985**, *66*, 23.
(17) Spiess, H. W. In *Developments in Oriented Polymers-1*; Ward, I. M., Ed.; Applied Science Publ.: London, 1982; p 47.
(18) Jelinski, L. W. *Annu. Rev. Mater. Sci.* **1985**, *15*, 359.
(19) Müller, K.; Meier, P.; Kothe, G. *Progr. NMR Spectroscop.* **1985**, *17*, 211.
(20) Ernst, R. R.; Bodenhausen, G.; Wokaun, A. *Principles of Nuclear Magnetic Resonance in One and Two Dimensions*; Clarendon Press: Oxford, 1987.
(21) (a) Schmidt, C.; Wefing, S.; Blümich, B.; Spiess, H. W. *Chem. Phys. Lett.* **1986**, *130*, 84. (b) Schmidt, C.; Blümich, B.; Spiess, H. W. *J. Magn. Reson.* **1988**, *79*, 269.
(22) (a) Wefing, S.; Spiess, H. W. *J. Chem. Phys.* **1988**, *89*, 1219. (b) Wefing, S.; Kaufmann, S.; Spiess, H. W. *J. Chem. Phys.* **1988**, *89*, 1234. (c) Kaufmann, S.; Wefing, S.; Schaefer, D.; Spiess, H. W. *J. Chem. Phys.* **1990**, *93*, 197.
(23) Hagemeyer, A.; Schmidt-Rohr, K.; Spiess, H. W. *Adv. Magn. Reson.* **1989**, *13*, 85.
(24) deJong, A. F.; Kentgens, A. P. M.; Veeman, W. S. *Chem. Phys. Lett.* **1984**, *109*, 337.
(25) Maricq, M. M.; Waugh, J. S. *J. Chem. Phys.* **1979**, *70*, 3300.
(26) (a) Harbison, G. S.; Spiess, H. W. *Chem. Phys. Lett.* **1986**, *124*, 128. (b) Harbison, G. S.; Vogt, V. D.; Spiess, H. W. *J. Chem. Phys.* **1987**, *86*, 1206. (c) Tang, P.; Santos, R. A.; Harbison, G. *Adv. Magn. Reson.* **1989**, *13*, 225. (d) Vogt, V. D.; Dettenmaier, M.; Spiess, H. W.; Pietralla, M. *Colloid Polym. Sci.* **1990**, *268*, 22.
(27) Abragam, A. *The Principles of Nuclear Magnetism.* Clarendon Press: Oxford, 1961, pp 138,139.
(28) Havens, J. R.; VanderHart, D. L. *Macromolecules* **1985**, *18*, 1663.
(29) Caravatti, P.; Neuenschwander, P.; Ernst, R. R. *Macromolecules* **1986**, *19*, 1895.
(30) (a) Schnabel, B.; Haubenreisser, U.; Scheler, G.; Müller, R. *Proc. 19th Congr. Ampere Magn. Reson. Relat. Phenom.* **1976**, 414. (b) Gerstein, B. C.; Pembleton, R. G.; Wilson, R. D.; Ryan, L. J. *J. Chem. Phys.* **1977**, *66*, 361. (c) Maciel, G. E.; Bronnimann, C. E.; Hawkins, B. L. *Adv. Magn. Reson.* **1990**, *14*, 125.
(31) Schmidt-Rohr, K.; Clauss, J.; Blümich, B.; Spiess, H. W. *Magn. Reson. Chem.* **1990**, *28*, S3.
(32) (a) Gall, C. M.; DiVerdi, J. A.; Opella, S. J. *J. Am. Chem. Soc.* **1981**, *103*, 5039. (b) Kinsey, R. A.; Agustin, K.; Oldfield, E. *J. Biol. Chem.* **1981**, *256*, 9028. (c) Rice, D. M.; Wittebort, R. J.; Griffin, R. G.; Meirovitch, E.; Stimson, E. R.; Meinwald, Y. C.; Freed, J. H.; Scheraga, H. A. *J. Am. Chem. Soc.* **1981**, *103*, 7707.
(33) (a) Spiess, H. W. *Colloid Polym. Sci.* **1983**, *261*, 193. (b) Wehrle, M.; Hellmann, G. P.; Spiess, H. W. *Colloid Polym. Sci.* **1987**, *265*, 193. (c) Jones, A. A. in ref 7, p 247.
(34) (a) Vold, R. L.; Vold, R. R.; Heaton, N. J. *Adv. Magn. Reson.* **1989**, *13*, 17. (b) Davis, J. H. *Adv. Magn. Reson.* **1989**, *13*, 195.
(35) Olejniczak, E. T.; Vega, S.; Griffin, R. G. *J. Chem. Phys.* **1984**, *81*, 4804.
(36) Herzfeld, J.; Berger, A. E. *J. Chem. Phys.* **1980**, *73*, 6021.
(37) Blümich, B.; Spiess, H. W. *Angew. Chem., Int. Ed. Engl.* **1988**, *27*, 1655.
(38) Aue, W. P.; Ruben, D. J.; Griffin, R. G. *J. Chem. Phys.* **1984**, *80*, 1729.
(39) (a) Alla, M. A.; Kundla, E. I.; Lippmaa, E. T. *JETP Lett.* **1978**, *27*, 194. (b) Yarim-Agaev, Y.; Tutunjian, P. N.; Waugh, J. S. *J. Magn. Reson.* **1982**, *47*, 51. (c) Bax, A.; Szeverenyi, N. M.; Maciel, G. E. *J. Magn. Reson.* **1983**, *51*, 400.
(40) Maciel, G. E.; Szeverenyi, N. M.; Sardashti, M. *J. Magn. Reson.* **1983**, *55*, 494.
(41) Terao, T.; Miura, H.; Saika, A. *J. Chem. Phys.* **1986**, *85*, 3816.
(42) Kolbert, A. C.; Griffin, R. G. *Chem. Phys. Lett.* **1990**, *166*, 87.
(43) (a) Dixon, W. T. *J. Chem. Phys.* **1982**, *77*, 3816. (b) Dixon, W. T.; Schaefer, J.; Sefcik, M. D.; Stejskal, E. O.; McKay, R. A. *J. Magn. Reson.* **1982**, *49*, 431.
(44) (a) Raleigh, D. P.; Olejniczak, E. T.; Vega, S.; Griffin, R. G. *J. Magn. Reson.* **1987**, *72*, 238. (b) Raleigh, D. P.; Kolbert, A. C.; Griffin, R. G. *J. Magn. Reson.* **1990**, *89*, 1. (c) Hagemeyer, A.; van der Putten, D.; Spiess, H. W. *J. Magn. Reson.* **1991**, *92*, 628.
(45) Tycko, R.; Dabbagh, G.; Mirau, P. A. *J. Magn. Reson.* **1989**, *85*, 265.
(46) Waugh, J. S. *Proc. Natl. Acad. Sci. USA* **1976**, *73*, 1394.
(47) Linder, M.; Höhener, A.; Ernst, R. R. *J. Chem. Phys.* **1980**, *73*, 4959.
(48) (a) Munowitz, M. G.; Griffin, R. G.; Bodenhausen, G.; Huang, T. H. *J. Am. Chem. Soc.* **1981**, *103*, 2529. (b) Munowitz, M. G.; Griffin, R. G. *J. Chem. Phys.* **1982**, *76*, 2848. (c) Munowitz, M. G.; Aue, W. P.; Griffin, R. G. *J. Chem. Phys.* **1982**, *77*, 1686.
(49) (a) Schaefer, J.; Sefcik, M. D.; Stejskal, E. O.; McKay, R. A.; Dixon, W. T.; Cais, R. E. *Macromolecules* **1984**, *17*, 1107. (b) Schaefer, J.; Stejskal, E. O.; McKay, R. A.; Dixon, W. T. *Macromolecules* **1984**, *17*, 1479. (c) Schaefer, J.; Stejskal, E. O.; Perchak, D.; Skolnick, J.; Yaris, R. *Macromolecules* **1985**, *18*, 368.
(50) Chirlian, L. E.; Opella, S. J. *Adv. Magn. Reson.* **1990**, *14*, 183.
(51) Naki, T.; Ashida, J.; Terao, T. *J. Chem. Phys.* **1988**, *88*, 6049.
(52) Kolbert, A. C.; deGroot, H. J. M.; Oas, T. G.; Griffin, R. G. *Adv. Magn. Reson.* **1989**, *13*, 183.
(53) Gullion, T.; Schaefer, J. *Adv. Magn. Reson.* **1989**, *13*, 57.
(54) Levitt, M. H.; Raleigh, D. P.; Creuzet, F.; Griffin, R. G. *J. Chem. Phys.* **1990**, *92*, 6347.
(55) (a) Gêny, F.; Monnerie, L. J. *J. Polym. Sci., Polym. Phys. Ed.* **1979**, *17*, 131, 147. (b) Rosenke, K.; Sillescu, H.; Spiess, H. W. *Polymer* **1980**, *21*, 757.
(56) Helfand, E.; Wassermann, Z. R.; Weber, T. B.; Skolnick, J.; Runnels, J. R. *J. Chem. Phys.* **1971**, *75*, 4441.
(57) Hirschinger, J.; Schaefer, D.; Spiess, H. W.; Lovinger, A. J. *Macromolecules* **1991**, *24*, 2428.
(58) Lovinger, A. J. In *Developments in Crystalline Polymers-1*; Basset, C. D., Ed.; Applied Science Publ.: London, 1981; p 195.
(59) Hagemeyer, A.; Brombacher, L.; Schmidt-Rohr, K.; Spiess, H. W. *Chem. Phys. Lett.* **1990**, *167*, 583.
(60) Pschorn, U.; Rössler, E.; Sillescu, H.; Kaufmann, S.; Schaefer, D.; Spiess, H. W. *Macromolecules* **1991**, *24*, 398.
(61) Schaefer, D.; Spiess, H. W.; Suter, U. W.; Fleming, W. W. *Macromolecules* **1990**, *23*, 3431.
(62) Vallerien, S. U.; Werth, M.; Kremer, F.; Spiess, H. W. *Liq. Cryst.* **1990**, *8*, 889.

(63) Kentgens, A. P. M.; deJong, A. F.; deBoer, E.; Veeman, W. S. *Macromolecules* **1985**, *18*, 1045.
(64) Zhang, C.; Wang, P.; Jones, A. A.; Inglefield, P. T.; Kambour, R. P. *Macromolecules* **1991**, *24*, 338.
(65) (a) Schmidt-Rohr, K.; Spiess, H. W. *25. Congress Ampere* Mehring, M., von Schütz, J. U., Wolf, H. C., Eds.; Springer-Verlag: Berlin, 1990; p 512. (b) Schmidt-Rohr, K.; Spiess, H. W. *Chem. Phys. Lett.* Submitted for publication.
(66) Schmidt-Rohr, K.; Spiess, H. W. *Phys. Rev. Lett.* **1991**, *66*, 3020.
(67) Schmidt-Rohr, K.; Spiess, H. W. *Macromolecules* **1991**, *24*, in press.
(68) Hoffmann, J. D.; Williams, G.; Passaglia, E. J. *J. Polym. Sci.* **1966**, *C14*, 173.
(69) Harbison, G. S.; Raleigh, D. P.; Herzfeld, J.; Griffin, R. G. *J. Magn. Reson.* **1985**, *64*, 284.
(70) (a) Borzo, M.; Zemke, K. Unpublished results. (b) Blümich, B.; Hagemeyer, A.; Schaefer, D.; Schmidt-Rohr, K.; Spiess, H. W. *Adv. Mater.* **1990**, *2*, 72.
(71) Yang, Y.; Hagemeyer, A.; Blümich, B.; Spiess, H. W. *Chem. Phys. Lett.* **1988**, *150*, 1.
(72) Yang, Y.; Hagemeyer, A.; Zemke, K.; Spiess, H. W. *J. Chem. Phys.* **1990**, *93*, 7740.
(73) Colombo, M. G.; Meier, B. H.; Ernst, R. R. *Chem. Phys. Lett.* **1988**, *146*, 189.
(74) Woodward, A. E. *Atlas of Polymer Morphology*; Hanser-Verlag: München, 1989.
(75) Packer, K. J.; Pope, J. M.; Yeung, R. R.; Cudby, M. E. A. *J. Polym. Sci., Polym. Phys. Ed.* **1984**, *22*, 589.
(76) Cheung, T. T. P.; Gerstein, B. C.; Ryan, L. M.; Taylor, R. E.; Dybowski, C. R. *J. Chem. Phys.* **1980**, *73*, 6059.
(77) Gerstein, B. C.; see ref 8, p 307.
(78) Caravatti, P.; Neuenschwander, P.; Ernst, R. R. *Macromolecules* **1985**, *18*, 119.
(79) Cudby, M. E. A.; Harris, R. K.; Metcalfe, K.; Packer, K. J.; Smith, P. W. R. *Polymer* **1985**, *26*, 169.
(80) Packer, K. J.; Poplett, I. J. F.; Taylor, M. J.; Vickers, M. E.; Whittaker, A. K.; Williams, K. P. J. *Makromol. Chem., Makromol. Symp.* **1990**, *34*, 161.
(81) Kitamaru, R.; Horii, F.; Murayama, K. *Macromolecules* **1986**, *19*, 636.
(82) Stejskal, E. O.; Schaefer, J.; Sefcik, M. D.; McKay, R. A. *Macromolecules* **1981**, *14*, 275.
(83) Zumbulyadis, N. *J. Magn. Reson.* **1983**, *53*, 486.
(84) Tekely, P.; Laupretre, F.; Monnerie, L. *Polymer* **1985**, *26*, 1081.
(85) Gobbi, G. C.; Silvestri, R.; Russell, T. P.; Lyerla, J. R.; Fleming, W. W.; Nishi, T. *J. Polym. Sci., Polym. Lett.* **1987**, *25*, 61.
(86) VanderHart, D. L. *Makromol. Chem., Macromol. Symp.* **1990**, *34*, 125.
(87) Linder, M.; Henrichs, P. M.; Hewitt, J. M.; Massa, D. J. *J. Chem. Phys.* **1985**, *82*, 1585.
(88) Henrichs, P. M.; Tribone, J.; Massa, D. J.; Hewitt, J. M. *Macromolecules* **1988**, *21*, 1282.
(89) (a) Andrew, E. R.; Bradbury, A.; Eades, R. G.; Wynn, T. *Phys. Lett.* **1963**, *4*, 99. (b) Andrew, E. R.; Farnell, L.; Gledhill, L. F.; Roberts, T. D. *Phys. Lett.* **1966**, *21*, 505.
(90) Schmidt-Rohr, K.; Clauss, J.; Blümich, B.; Spiess, H. W. *ACS Polym. Prepr.* **1990**, *31*, 172.
(91) Löwenhaupt, B.; Hellmann, G. P. *Colloid Polym. Sci.* **1990**, *268*, 885.
(92) Helfand, E.; Wassermann, Z. R. In *Developments in Block Copolymers-1*; Goodman, I., Ed.; Applied Science Publ.: London, 1982; Chapter 4.
(93) Henrichs, P. M.; Linder, M. *J. Magn. Reson.* **1984**, *58*, 458.
(94) Tycko, R.; Dabbagh, G. *J. Am. Chem. Soc.* **1991**, *113*, 3592.
(95) Raleigh, D. P.; Levitt, M. H.; Griffin, R. G. *Chem. Phys. Lett.* **1988**, *146*, 71.
(96) Raleigh, D. P.; Creuzet, F.; Das Dupta, S. K.; Levitt, M. H.; Griffin, R. G. *J. Am. Chem. Soc.* **1989**, *111*, 4502.
(97) Veeman, W. S.; Cory, D. G. *Adv. Magn. Reson.* **1989**, *13*, 43.
(98) Günther, E.; Blümich, B.; Spiess, H. W. *Mol. Phys.* **1990**, *71*, 477.